Received: 20 May 2020 | Revised: 1 September 2020 | Accepted: 30 September 2020

DOI: 10.1002/nag.3157

RESEARCH ARTICLE

WILEY

A cover-based contact detection approach for irregular convex polygons in discontinuous deformation analysis

Xiaoying Zhuang[1,2] | **Fei Zheng**[2] | **Hong Zheng**[3] | **Yu-Yong Jiao**[4] | **Timon Rabczuk**[5,6] | **Peter Wriggers**[7]

[1] Department of Geotechnical Engineering, College of Civil EngineeringTongji University, Shanghai, China

[2] Institute of Photonics, Faculty of Mathematics and PhysicsLeibniz University Hannover, Hannover, Germany

[3] Key Laboratory of Urban Security and Disaster Engineering (Beijing University of Technology), Ministry of Education, Beijing, China

[4] Faculty of Engineering, China University of Geosciences, Wuhan, PR China

[5] Division of Computational Mechanics, Ton Duc Thang University, Ho Chi Minh City, Vietnam

[6] Faculty of Civil Engineering, Ton Duc Thang University, Ho Chi Minh City, Vietnam

[7] Institute of Continuum Mechanics, Leibniz University Hannover, Hannover, Germany

Correspondence
Fei Zheng, Institute of Photonics, Faculty of Mathematics and Physics, Leibniz University Hannover, 30167 Hannover, Germany.
Email: fzheng@hot.uni-hannover.de
Timon Rabczuk
Email: timon.rabczuk@tdtu.edu.vn

Funding information
National Natural Science Foundation of China, Grant/Award Numbers: 51479191, 11672360; Alexander von Humboldt-Stiftung

Abstract

Irregular polygon shapes (eg, with small edges or small angles) are usually encountered in the contact simulation of discrete block systems. Treatment of irregular polygons in contact detection process has critical effects on the robustness and efficiency of the discontinuous computation approach. The present work proposes a cover-based strategy to detect and solve contacts of irregular convex polygons in a robust and efficient way. Contact constraints of two polygons are represented by vertex-edge and edge-vertex contact covers in 2D. Two loops, namely vertex-edge loop and edge-vertex loop, and two filter criteria, namely the entrance filter criterion and the distance filter criterion, are used to establish the potential contact cover list of two neighbor polygons. The initial active and closed contact covers are chosen based on block configuration at the beginning of the step and they are then updated in the open-close iteration process using proposed criteria. This strategy is implemented in discontinuous deformation analysis. The robustness of the proposed cover-based approach and the conventional type-based approach in handling contact of irregular blocks is verified first. Then, the contact analysis efficiency of the cover-based approach with different contact tolerances is evaluated. This cover-based method can be extended to 3D case for efficient and robust contact analysis of irregular polyhedral blocks.

KEYWORDS
contact cover, discontinuous deformation analysis, entrance block, irregular polygon, small angle, small edge

Highlights

- Robust contact treatment of irregular convex polygons with small edges or small angles.
- Efficient contact analysis of irregular convex polygons with good accuracy.
- Good performance in all testing examples including irregular shaped blocks.

1 | INTRODUCTION

Contact mechanics has its application in many engineering problems,[1,2] and specially, one has to solve the contact of an assembly of discrete bodies in many geotechnical engineering problems.[3–9] Some commonly applied numerical approach for fracture and contact analysis of rock and soil material includes the finite element method,[10] the phase field approach,[11] peridynamics,[12] the discrete element method,[13] discontinuous deformation analysis (DDA),[14,15] distinct lattice spring method,[16] rigid block spring method,[17] the combined finite-discrete element method,[18] and the numerical manifold method.[19–21] Solving contact interaction of assembly of discrete bodies is a challenging task considering the computational efficiency and the algorithmic robustness in detecting and solving contact of massive particles/blocks with various shapes.[22–30] A two-phase process, that is, neighbor search and delicate search, is commonly used to improve the detection efficiency. For a system involving a lot of blocks/particles, the efficiency of establishing neighbor block pairs and resolving geometrical constraint in contact detection has been greatly improved by several algorithms, such as no-binary search algorithm,[31] double-ended spatial sorting algorithm,[32] C-Grid method,[33] multicover algorithm.[22,23]

Polygonal and polyhedral block/particle shapes are commonly used to represent the geometries of rock masses or rock grains. Specially, irregular polygonal or polyhedral block/particle with small edges or sharp angles can be encountered considering intersection of joints[34,35] and geological formation of mesoscale rock grains.[36,37] The efficiency and robustness of the detection algorithm in resolving the geometrical constraints for two neighbor blocks/particles are crucial factors for successful application. Contact of two bodies may involve the physical process of separation to contact, contact to separation, and switch of different contact modes. It is necessary to measure their distance and establish the geometrical relationship in all contact scenarios for successful contact interaction simulation. Both explicit and implicit schemes have been applied to solve contact problem,[38–46] where contact constraints and associated physical states should be obtained and updated by the contact detection and solution process in all analysis steps. For the explicit schemes, the contact force with its acting position for specific instant is needed in computation of the acceleration term. By contrast, for implicit schemes, such as DDA with constant acceleration integration solution module, the geometrical constraints and associated physical states are established with the initial configuration at the beginning of each step, and in each step, the converged constraints and physical states are obtained with a trial-and-error procedure named open-close iteration (OCI).[47,48]

Assume the displacement of contacting bodies is limited within a computation step, contact constraints of two polygons can be established in a "local" way, where different contact types are used to describe the contact constraints.[14] For 2d polygons, vertex-to-vertex and vertex-to-edge are used[49] and for 3d polyhedra, vertex-to-vertex, vertex-to-edge, vertex-to-face, and edge-to-edge are used.[50,51] For these type-based contact solution approaches, some tolerances (ie, contact tolerance and entrance tolerance) are used in the identification of contact types, and their values are associated with the maximum step displacement and the maximum rotation angle. To recognize contact types of polygons, two commonly used contact territory definitions are illustrated in Figures 1 and 2. For these approaches, the robustness and computational efficiency during contact analysis is affected by the adopted contact tolerances and the polygon shapes.

For contact analysis of polygonal and polyhedral block systems, there are some common issues related to the block shape. These include the nonsmooth changes of contact normal, determination of contact pair encountering quasi-parallel edges/faces cases, and algorithmic robustness and computational efficiency in treating irregular polygonal blocks with small edges or small angles. The nonsmooth changes of contact normal for polygon and polyhedron contact problems have been investigated, and several algorithms have been proposed to solve this issue within the explicit solution framework, such as the corner rounding scheme,[52,53] the potential particle method,[54,55] the energy conservation method,[56] and the potential function method.[4,57–61] The iterative methods in conventional DDA program can solve the polygon contact problems while remaining the nonsmooth feature in contact normal change.[62–65] The indeterminacy in solving vertex-vertex contact problems[66] and the algorithmic robustness problem[25] for contact analysis of quasi-parallel edges/faces pairs was also discussed.

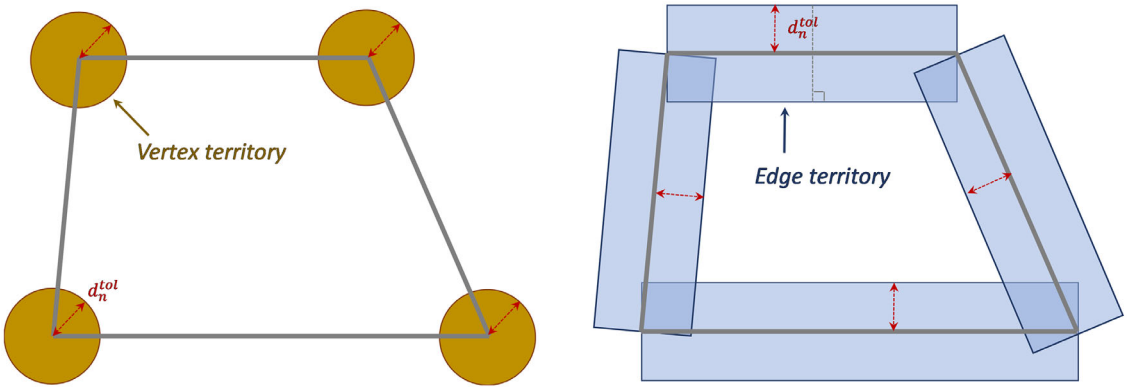

FIGURE 1 Illustrations of the vertex and edge contact search territories of the type-based contact detection with definition 1

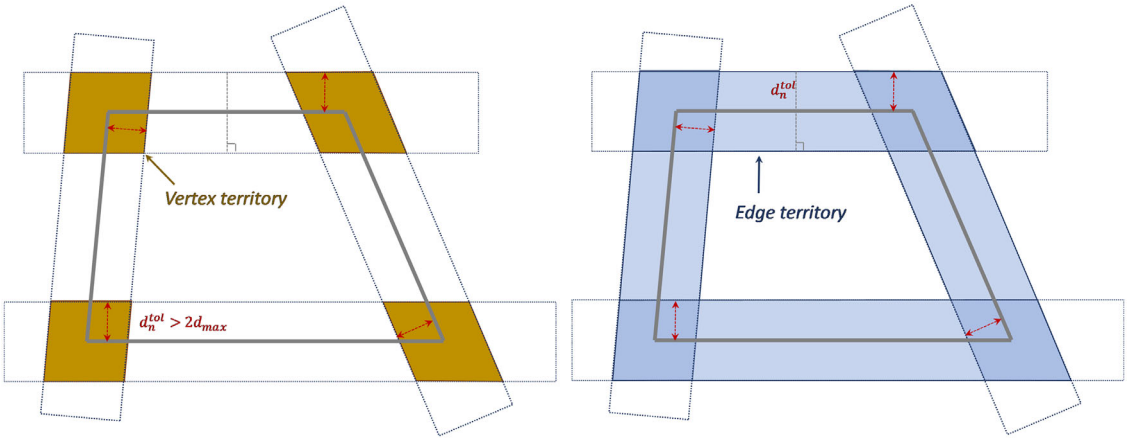

FIGURE 2 Illustrations of the vertex and edge contact search territories of the type-based contact detection with definition 2

In this paper, the robustness and efficiency in contact detection of "irregular" polygons are discussed, where "irregular" polygons represent the polygons with small edges or small angles, as illustrated in Figure 3. When irregular polygonal blocks with small edges or small angles are encountered, the type-based detection strategies may lead to the following robustness or efficiency issues: (1) inappropriate or replicated contact types when large contact tolerance is applied; (2) missing of appropriate contact types and associated large block penetration when small contact tolerance and small contact penalty value are used; and (3) more computation steps and low analysis efficiency when small contact tolerance and large penalty value are used.

To overcome above difficulties related to polygonal block shapes and take full advantages of using large time step for implicit solution methods, a cover-based detection approach that is based on the contact theory[67] is proposed. It establishes and solves contacts of polygons in a "global" way, avoiding the robust problems in traditional type-based detection approach encountering irregular convex polygons. Fundamentals and key algorithm of the proposed approach are presented in Section 2. A brief view of the formulation and analysis procedure of DDA is shown in Section 3. The robustness

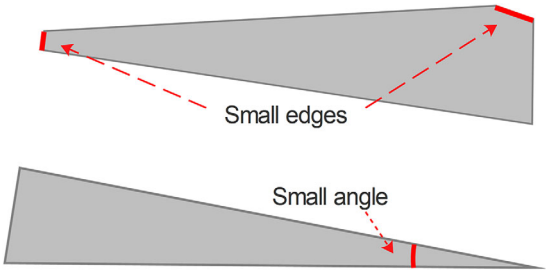

FIGURE 3 Irregular polygons with small edges and small angles

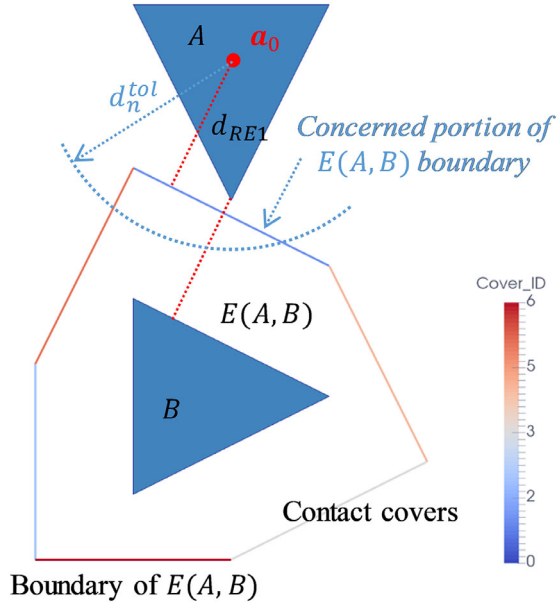

FIGURE 4 An illustration of the concepts of cover-based approach

verification and efficiency evaluation of the propose approach in modeling contact of irregular polygons are discussed in Sections 4 and 5. Conclusions are made in Section 6.

2 | THEORY AND ALGORITHM OF THE COVER-BASED APPROACH

Contact detection approaches aim to capture kinematic constraints of a discrete block systems, which includes the state changes between separation and contact, and contact mode changes between locked and slip. A major challenge of the contact detection approach is its robustness (accuracy and efficiency) in treating irregular blocks with small angles or small edges, which is commonly encountered in rock block systems formed by the intersection of several joint sets and excavations.

Given the drawbacks of the type-based contact detection algorithms in handling irregular blocks, the cover-based contact detection approach is proposed to establish the geometrical constraints and determine the contact mode of convex polygonal blocks in each analyzing step. This approach is based on the concepts and theories on entrance block and contact cover,[67] which provide the following methodology to detect contact of polygons as illustrated in Figure 4: (1) definition of entrance block transfers contact of two blocks to that of a reference point and an entrance block; (2) boundary of entrance block is an assembly of finite contact covers, each representing a vertex-edge pair; and (3) the "active" contact covers chosen by specific criteria (eg, the first entrance principle and the shortest exit principle) will be used for the penalty function formulation. Compared to the traditional type-based contact detection approaches, the cover-based strategy establishes a vertex-edge contact cover list globally for two blocks. It avoids the local differentiation of vertex-vertex and vertex-edge contact types, and thus eliminates the potential errors in the establishment of contact list for irregular blocks.

Both the kinetic behavior and quasi-static behavior of a block system are analyzed stepwise. As the global displacement is limited in each step, only a small set of contact covers corresponding to the local contact boundary is needed, and only the active covers are chosen for penalty function formulation. This section focuses on theories and algorithms of the proposed cover-based contact detection approach. Concepts of entrance block and contact cover, criteria of entrance filter and distance filter, strategies to determine contact cover activity, and the detection flowchart are given in the following subsections.

2.1 | Entrance block

The following mathematical symbols are used in descriptions of entrance block and contact cover. A, B are two polygonal blocks, and ∂A, ∂B are the boundaries of blocks A, B, respectively. $\boldsymbol{a}_i = (x_i, y_i)$, $\boldsymbol{b}_j = (x_j, y_j)$ are 2D points. $\boldsymbol{b}_j\boldsymbol{b}_{j+1}$ is an edge from point $\boldsymbol{b}_j$ to point $\boldsymbol{b}_{j+1}$, $\boldsymbol{a}_i \sim \boldsymbol{b}_j\boldsymbol{b}_{j+1}$ is the combination of vertex $\boldsymbol{a}_i$ and edge $\boldsymbol{b}_j\boldsymbol{b}_{j+1}$.

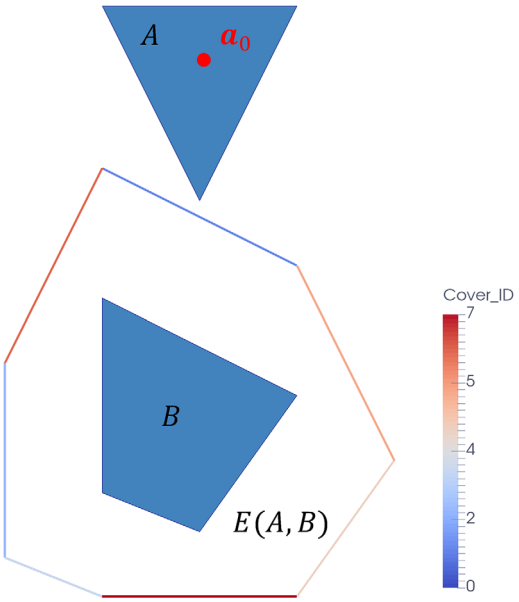

FIGURE 5 An example of the entrance block of a triangle and a quadrangle

Choosing a reference point $\boldsymbol{a}_0$, the entrance block $E(A,B)$ for blocks A and B is defined by:[67–69]

$$E(A,B) = B - A + \boldsymbol{a}_0 = \cup_{\boldsymbol{a}\in A, \boldsymbol{b}\in B}(\boldsymbol{b} - \boldsymbol{a} + \boldsymbol{a}_0). \tag{1}$$

If blocks A and B are polygons, $E(A,B)$ is a polygon. If blocks A and B are convex, $E(A,B)$ is convex. Using the concept of entrance block, the contact relationship between two polygons A and B can be equivalently represented by the contact relationship between the reference point $\boldsymbol{a}_0$ and the entrance block $E(A,B)$. Figure 5 shows an example of entrance block obtained with a triangle and a quadrangle.

The distance d_{RE} between the reference point and the entrance block here is defined by:

$$d_{RE} = min\{|\boldsymbol{a}_0 - \boldsymbol{x}_e|, \forall \boldsymbol{x}_e \in E(A,B)\}. \tag{2}$$

$d_{RE} > 0$ indicates blocks A and B are detached, while $d_{RE} = 0$ indicates blocks A and B are in contact or overlapping. Note that the point number in point set $E(A,B)$ is infinite. A more convenient way to measure the distance is to use the reference point and the boundary of the entrance block instead of the whole domain. The distance d_{RE1} between the reference point and the entrance block boundary $\partial E(A,B)$ is defined by:

$$d_{RE1} = min\{|\boldsymbol{a}_0 - \boldsymbol{x}_e|, \forall \boldsymbol{x}_e \in \partial E(A,B)\}. \tag{3}$$

$d_{RE1} > 0$ indicates the reference point may be inside or outside of the entrance block. If the reference point is outside, d_{RE1} indicates shortest distance to entrance it; if the reference point is inside, d_{RE1} indicates shortest distance to exit it. $d_{RE1} = 0$ indicates that blocks A and B contact each other.

2.2 | Establishment of contact cover

Denote $C(0,1)$ as the union of all contact edges with the form $E(\boldsymbol{a}_i, \boldsymbol{b}_j\boldsymbol{b}_{j+1})$, $C(0,1) = \bigcap_{contact\ edge} E(\boldsymbol{a}_i, \boldsymbol{b}_j\boldsymbol{b}_{j+1})$. Similarly, $C(1,0)$ is denoted as union of all contact edges with the form $E(\boldsymbol{a}_i\boldsymbol{a}_{i+1}, \boldsymbol{b}_j)$, $C(1,0) = \bigcap_{contact\ edge} E((\boldsymbol{a}_i\boldsymbol{a}_{i+1}, \boldsymbol{b}_j)$. Here, $\boldsymbol{a}_i$, $\boldsymbol{a}_i\boldsymbol{a}_{i+1}$, $\boldsymbol{b}_j$, $\boldsymbol{b}_j\boldsymbol{b}_{j+1}$ represent vertices and edges from blocks A and B, respectively. $C(0,1)$ and $C(1,0)$ are named contact covers of vertex-edge pairs and edge-vertex pairs, respectively. The theorem of contact edges of 2D convex blocks is[67]

$$\partial E(A,B) = C(0,1) \cup C(1,0). \tag{4}$$

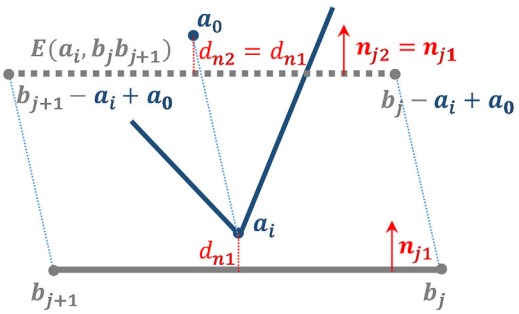

FIGURE 6 Illustrations of the computation of $E(\boldsymbol{a}_i, \boldsymbol{b}_j\boldsymbol{b}_{j+1})$

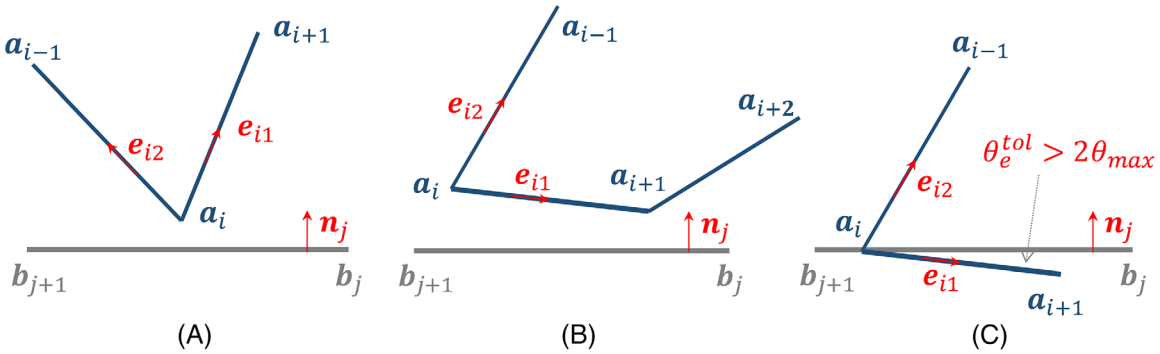

FIGURE 7 Illustrations for the entrance filter criterion: (A) relationship of $\boldsymbol{e}_i$ and $\boldsymbol{n}_j$; (B) a quasi-parallel edge case; and (C) the meaning of θ_e^{tol}

This theorem shows that the boundary of the entrance block can be constructed with contact covers formed by $\boldsymbol{a}_i \sim \boldsymbol{b}_j\boldsymbol{b}_{j+1}$ pairs and $\boldsymbol{a}_i\boldsymbol{a}_{i+1} \sim \boldsymbol{b}_j$ pairs. The boundary of an entrance block is a finite cover system. Each cover indicating the geometrical information of a contact constraint and it is named a contact cover.

It should be noted that only a portion of vertex-edge ($\boldsymbol{a}_i \sim \boldsymbol{b}_j\boldsymbol{b}_{j+1}$) and edge-vertex ($\boldsymbol{a}_i\boldsymbol{a}_{i+1} \sim \boldsymbol{b}_j$) pairs those satisfies the filter criteria will form the contact covers for two polygons. Contact cover can be computed with Equation (1) by setting blocks A and B as boundary vertices or edges of two polygons. Figure 6 illustrates the computation process of $E(\boldsymbol{a}_i, \boldsymbol{b}_j\boldsymbol{b}_{j+1})$.

For convex polygons, all contact covers, $C(0, 1)$ and $C(1, 0)$, form boundaries of the entrance block. For concave polygons, it might be complex to obtain the accurate boundary of entrance block as some redundant parts need to be cut.[69] This paper focuses on convex polygons and it is assumed that a concave polygon can be equivalently represented by a subset of convex ones. The contact theory[67] demonstrates that the choice of the reference point has no effects on the measurement of the geometrical relationship (eg, distance and geometry information of contact) of two polygons. The calculation of the normal distance and the judgment of the geometrical position between the reference point and the contact cover (vertex-edge and edge-vertex) can be proceeded by associated vertices and edges with their original coordinate format.

2.2.1 | The entrance filter criterion

The entrance filter criterion is used to determine the eligibility of vertex-edge and edge-vertex pairs in forming a contact cover according to their geometrical configuration.[14,25,49,51] For a vertex-edge pair $\boldsymbol{a}_i \sim \boldsymbol{b}_j\boldsymbol{b}_{j+1}$, all the unit vectors e_i along the edge that joining the vertex $\boldsymbol{a}_i$ should point outward of the edge $\boldsymbol{b}_j\boldsymbol{b}_{j+1}$, as shown in Figure 7A. Considering the quasi-parallel cases,[25] the entrance filter criterion for $\boldsymbol{a}_i \sim \boldsymbol{b}_j\boldsymbol{b}_{j+1}$ is represented by:

$$\boldsymbol{e}_i \cdot \boldsymbol{n}_j > -\sin\left(\theta_e^{tol}\right), \tag{5}$$

where $\boldsymbol{n}_j$ represents the unit normal vector of edge $\boldsymbol{b}_j\boldsymbol{b}_{j+1}$ that point outward of block B, θ_e^{tol} represents the allowed overlapping angle. Here, θ_e^{tol} is introduced to capture the vertex-edge pairs in contact scenario that two edges are in

quasi-parallel condition, as shown in Figure 7B. This overlapping angle tolerance should be twice of the maximum rotation angle (θ_{max}) in each step to capture all potential vertex-edge and edge-vertex pairs. The meaning of θ_e^{tol} is illustrated in Figure 7C.

Similarly, for an edge-vertex pair $\boldsymbol{a}_i\boldsymbol{a}_{i+1} \sim \boldsymbol{b}_j$, all the unit vectors $\boldsymbol{e}_j$ along the edges joining the vertex $\boldsymbol{b}_j$ should point outward of the edge $\boldsymbol{a}_i\boldsymbol{a}_{i+1}$,

$$\boldsymbol{e}_j \cdot \boldsymbol{n}_i > -\sin\left(\theta_e^{tol}\right), \tag{6}$$

where n_i represents the unit normal vector of edge a_ia_{i+1} that point outward of block A.

Using the cover-based representation methods, the differentiation of contact types (eg, vertex-to-vertex, vertex-to-edge, and edge-to-edge) in contact detection phase is not necessary, as contact information can be represented completely by vertex-edge and edge-vertex contact covers. Establishing the geometrical constraints with the contact covers of vertex-edge and edge-vertex pairs is enough for contact simulation. As a result, contact detection can be proceeded with only vertex-edge (and edge-vertex) loops and the cover-based representation method can avoid the difficulties in differentiating different contact types encountering polygonal block with small edges.

2.2.2 | The distance filter criterion

The target of contact detection approach is to establish the geometrical constraints in an efficient way. Using the entrance block theory, the geometrical relationship of two polygons can be equivalently evaluated by the relationship of the chosen reference points and the established entrance block. Note that in a realistic scenario, contact only occurs on a small portion of the two approaching polygons. This contact area can be mapped to a local area of entrance block boundary, which consists of finite contact covers. On this basis, only a small group of the contact covers those close to the reference point are necessary in the establishment of the geometrical constraints in a step. Therefore, a new distance filter criterion is proposed to exclude the contact covers those are far from the contact area.

The distance filter criterion is used to find the geometrical element pair that is close to each other.[14,25] For two-dimensional polygonal blocks, this is to judge if a vertex and an edge are close enough to contact during the analysis step. The perpendicular distances d_{ij}^n of vertex $\boldsymbol{a}_i$ to edge $\boldsymbol{b}_j\boldsymbol{b}_{j+1}$, the projection ratio r_{ij} of vertex $\boldsymbol{a}_i$ on edge $\boldsymbol{b}_j\boldsymbol{b}_{j+1}$, and the distance d_{ij}, $d_{i(j+1)}$ of vertex $\boldsymbol{a}_i$ to edge nodes $\boldsymbol{b}_j$ and $\boldsymbol{b}_{j+1}$ are used for the filter judgment of vertex-edge pair $\boldsymbol{a}_i \sim \boldsymbol{b}_j\boldsymbol{b}_{j+1}$. The perpendicular distance d_{ij}^n of vertex $\boldsymbol{a}_i$ to edge $\boldsymbol{b}_j\boldsymbol{b}_{j+1}$ is computed by:

$$d_{ij}^n = \left(\boldsymbol{a}_i - \boldsymbol{b}_j\right) \cdot \boldsymbol{n}_j. \tag{7}$$

The projection ratio r_{ij} of vertex $\boldsymbol{a}_i$ on edge $\boldsymbol{b}_j\boldsymbol{b}_{j+1}$ is computed by:

$$r_{ij} = \frac{\left(\boldsymbol{a}_i - \boldsymbol{b}_j\right) \cdot \left(\boldsymbol{b}_{j+1} - \boldsymbol{b}_j\right)}{\left(\boldsymbol{b}_{j+1} - \boldsymbol{b}_j\right) \cdot \left(\boldsymbol{b}_{j+1} - \boldsymbol{b}_j\right)}. \tag{8}$$

The distance d_{ij} of vertex $\boldsymbol{a}_i$ to edge nodes $\boldsymbol{b}_j$ is computed by:

$$d_{ij} = \left|\boldsymbol{a}_i - \boldsymbol{b}_j\right| = \sqrt{\left(x_i - x_j\right)^2 + \left(y_i - y_j\right)^2}. \tag{9}$$

The distance $d_{i(j+1)}$ of vertex $\boldsymbol{a}_i$ to edge nodes $\boldsymbol{b}_{j+1}$ can be computed in the same way with Equation (9).

As shown in Figure 8, the contact region $\Omega_{j(j+1)}^C$ of edge $\boldsymbol{b}_j\boldsymbol{b}_{j+1}$ is the union of point (p_i) from three subregions $\Omega_{j(j+1)}^{C1}$, $\Omega_{j(j+1)}^{C2}$, and $\Omega_{j(j+1)}^{C3}$:

$$\Omega_{j(j+1)}^{C1} = \left\{ \boldsymbol{p}_i \middle| \left|d_{ij}^n\right| \le d_n^{tol} \text{ and } r_{ij} \in [0,1] \right\}, \tag{10a}$$

$$\Omega_{j(j+1)}^{C2} = \left\{ \boldsymbol{p}_i \middle| d_{ij} \le d_n^{tol} \right\}, \tag{10b}$$

$$\Omega_{j(j+1)}^{C3} = \left\{ \boldsymbol{p}_i \middle| d_{i(j+1)} \le d_n^{tol} \right\}, \tag{10c}$$

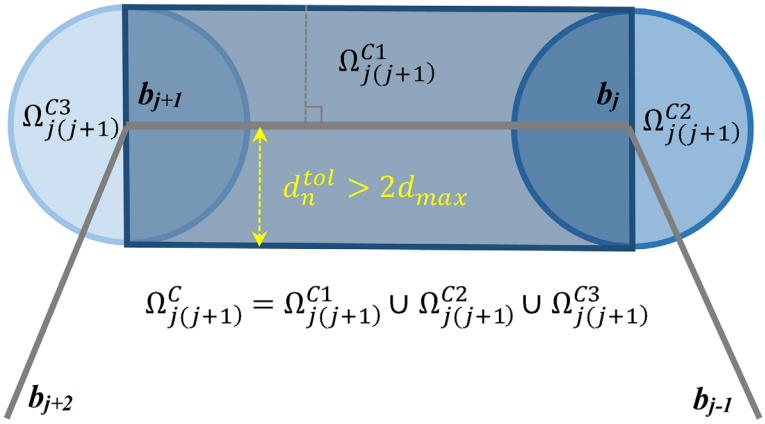

FIGURE 8 The contact region of edge $\boldsymbol{b}_j\boldsymbol{b}_{j+1}$

where d_n^{tol} is the input contact tolerance to determine the valid contact region of an edge. If vertex $\boldsymbol{a}_i$ is inside the contact region $\Omega^C_{j(j+1)}$ of edge $\boldsymbol{a}_i \sim \boldsymbol{b}_j\boldsymbol{b}_{j+1}$ described by Equation (10), the contact cover of $\boldsymbol{a}_i \sim \boldsymbol{b}_j\boldsymbol{b}_{j+1}$ passes the distance filter and it will be added to be contact cover list C^L.

The distance filter criterion for edge-vertex pair $\boldsymbol{a}_i\boldsymbol{a}_{i+1} \sim \boldsymbol{b}_j$ can be obtained by switching $\boldsymbol{a}_i$ to $\boldsymbol{b}_j$, $\boldsymbol{b}_j\boldsymbol{b}_{j+1}$ to $\boldsymbol{a}_i\boldsymbol{a}_{i+1}$ in Equations (7-10). Similarly, if the vertex $\boldsymbol{b}_j$ is inside the contact region $\Omega^C_{i(i+1)}$ of edge $\boldsymbol{a}_i\boldsymbol{a}_{i+1}$, the contact cover $\boldsymbol{a}_i\boldsymbol{a}_{i+1} \sim \boldsymbol{b}_j$ will be added to the contact cover list C^L.

2.3 | Activity and states of contact cover

The vertex-edge ($\boldsymbol{a}_i \sim \boldsymbol{b}_j\boldsymbol{b}_{j+1}$) and edge-vertex ($\boldsymbol{a}_i\boldsymbol{a}_{i+1} \sim \boldsymbol{b}_j$) pairs those pass the distance and entrance filter criterion will form the contact cover list C^L, that is, the concerned portion of the entrance block boundaries. During the contact interaction simulation, only the "active" and "closed" (locked and slip) contact covers will be used to establish the contact constraints. In this paper, the "active" contact cover means the valid portion of C^L for the formulations at current simulation step. When the reference point is inside the entrance block, the contact covers with the shortest exiting route are active. When the reference point is outside and tends to move inside of the entrance block, the contact covers those are intersected with the moving trajectory of the reference point are active.

For an active contact cover $\boldsymbol{a}_i \sim \boldsymbol{b}_j\boldsymbol{b}_{j+1}$, the vertex $\boldsymbol{a}_i$ and its projection point $\boldsymbol{p}_j$ on the edges are recognized as two contact points; the normal vector of the edge $\boldsymbol{b}_j\boldsymbol{b}_{j+1}$ (point from block B to block A) is recognized as the contact normal direction $\boldsymbol{n}_j$. One of the vectors ($\boldsymbol{b}_j - \boldsymbol{b}_{j+1}$ *or* $\boldsymbol{b}_{j+1} - \boldsymbol{b}_j$), which corresponds to relative sliding velocity ($\boldsymbol{v}_{ai} - \boldsymbol{v}_{pj}$), is chosen as initial tangent sliding direction $\boldsymbol{t}_j$.

The analysis of the discrete block system follows a step-by-step analysis process. In each analysis step, the contact cover list C^L can be established with the block configuration at the beginning of current step. However, the activity and the contact states of each contact cover may change during the analysis period. The initial active contact covers are selected in the contact cover list C^L and their contact states are determined according to the initial configuration, initial velocity, and their states at the end of previous step. OCI is then applied to obtain the realistic active contact cover and the converged contact states in current analysis step.[14]

As indicated in Ref. 67, the entrance block of two polygons is still a polygon. Moreover, the entrance block is convex if the two polygons are both convex. As only convex polygons are considered, these selected contact covers C^L from two convex blocks then form a portion of the boundaries of a convex block. This convex feature can be used in the determination of active contact covers.

2.3.1 | Determination scheme at step beginning

At the beginning of each time step, the active contact covers and associated contact states will be assumed or inherited from previous step. The determination of active contact cover at the beginning of the step is based on distance of the reference point to the entrance block. For two convex polygons, measurement of the distance d_{RE2} from the reference

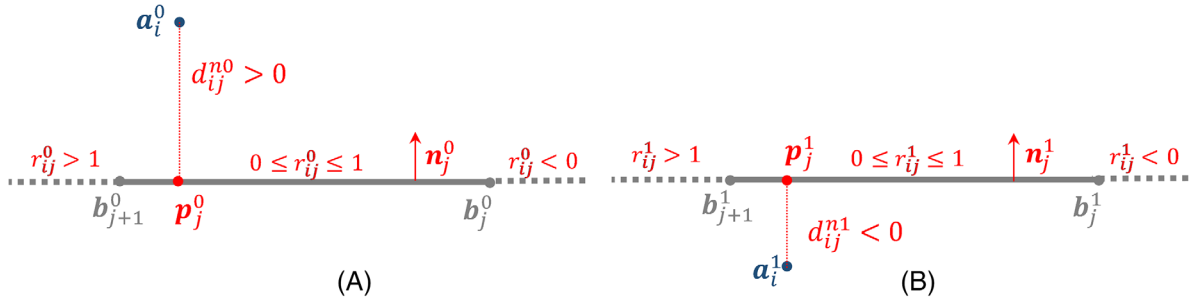

FIGURE 9 Illustrations for the computation of r_{ij} and d_{ij}^n: (A) at instant t^0; and (B) at instant t^1

point to the entrance block boundary based on established contact covers is defined by:

$$d_{RE2} = max\left\{d_k^n\left(C_k\right), \forall C_k \in C^L\right\}, \tag{11}$$

where d_k^n represents the perpendicular distance of the kth vertex-edge contact cover C_k in the established contact cover list C^L. Here, d_k^n of a contact cover is computed by Equation (7). The contact covers corresponding to d_{RE2} will be selected for further consideration. If the reference point is outside of the entrance block, d_{RE2} denotes the closest normal distance to enter the entrance block; if the reference point is inside the entrance block, d_{RE2} denotes the closest normal distance to exit the entrance block. For all contact covers corresponding to d_{RE2}, the projection ratio r_{ij} will be used to determine the initial activity. If $r_{ij} \in [0, 1]$, the contact cover is active.

For frictionless problems, the state of a contact cover $\boldsymbol{a}_i \sim \boldsymbol{b}_j\boldsymbol{b}_{j+1}$ is open if $d_{ij}^n \ge 0$; the contact state is closed if $d_{ij}^n < 0$. For frictional but cohesionless problems, the "locked" and "sliding" states of a contact cover at the end of previous step will be transferred to the same contact cover in current step. If a contact cover $\boldsymbol{a}_i \sim \boldsymbol{b}_j\boldsymbol{b}_{j+1}$ is established at the first time, it is set to open if $d_{ij}^n \ge 0$; it will be set to locked if $d_{ij}^n < 0$. The converged contact states can be determined in OCI process. For cohesive and frictional problems, the difference is the existence of a cohesive strength for initial locked contact cover; once the locked states are broken, the cohesive strength is removed.

2.3.2 | Trajectory-tracking scheme in analysis cycles

Both the activity and states of contact cover can change during an analysis step. The active contact cover will change if (1) the reference point move from one contact cover to its adjacent contact covers or (2) the reference point move from outside to inside of the entrance block through some contact covers different from the initial assumed active contact covers. For case (1), the change of contact cover activity is naturally updated at the beginning of next time step according to the criterion by Equation (11) and their updated configuration. Case (2) can be mapped to the contact scenarios those including approaching vertices; for this case, the criterion by Equation (11) may not accurately reflect the realistic entrance path and thus introduce some perturbations to the results. For this condition, a trajectory-tracking strategy is proposed and applied in OCI process to capture the realistic active contact covers.

Assume $\boldsymbol{a}_i^0, \boldsymbol{b}_j^0, \boldsymbol{b}_{j+1}^0, \boldsymbol{a}_i^1, \boldsymbol{b}_j^1, \boldsymbol{b}_{j+1}^1$ are the coordinate vectors of vertex and edge boundaries at the beginning (t^0) and the end (t^1) of a computational step, respectively. The projection ratio r_{ij} of vertex $\boldsymbol{a}_i$ on edge $\boldsymbol{b}_j\boldsymbol{b}_{j+1}$, the normal distance d_{ij}^n from vertex $\boldsymbol{a}_i$ to edge $\boldsymbol{b}_j\boldsymbol{b}_{j+1}$ at t^0 (r_{ij}^0, d_{ij}^{n0}), and t^1 (r_{ij}^1, d_{ij}^{n1}) can be computed based on block configuration at t^0 and t^1, which is illustrated in Figure 9. A simple strategy is used to judge the intersection of the moving trajectories of vertex $\boldsymbol{a}_i$ and edge $\boldsymbol{b}_j\boldsymbol{b}_{j+1}$, based on r_{ij}^0, d_{ij}^{n0}, r_{ij}^1, d_{ij}^{n1}.

Here, the direction from $\boldsymbol{b}_j$ to $\boldsymbol{b}_{j+1}$ on the line $\boldsymbol{b}_j\boldsymbol{b}_{j+1}$ is defined as forward, and the direction from $\boldsymbol{b}_{j+1}$ to $\boldsymbol{b}_j$ is defined backward. The intersection point is on the forward direction of $\boldsymbol{b}_j$ in the following three cases:

$$r_{ij}^0 > 0 \; and \; r_{ij}^1 \ge 0, \tag{12a}$$

$$r_{ij}^0 > 0 \; and \; r_{ij}^1 < 0 \; and \; \left|\frac{r_{ij}^0}{r_{ij}^1}\right| \ge \left|\frac{d_{ij}^{n0}}{d_{ij}^{n1}}\right|, \tag{12b}$$

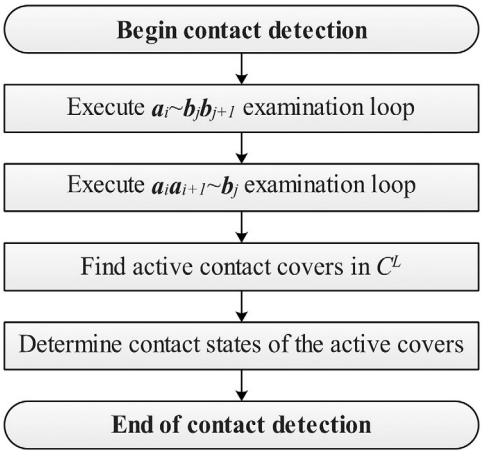

FIGURE 10 The flowchart of the proposed contact detection process

$$r_{ij}^0 \le 0 \text{ and } r_{ij}^1 > 0 \text{ and } \left|\frac{r_{ij}^0}{r_{ij}^1}\right| \le \left|\frac{d_{ij}^{n0}}{d_{ij}^{n1}}\right|. \tag{12c}$$

The intersection point is on the backward direction of $\boldsymbol{b}_{j+1}$ in the following three cases:

$$r_{ij}^0 > 1 \text{ and } r_{ij}^1 < 1 \text{ and } \left|\frac{r_{ij}^0 - 1}{r_{ij}^1 - 1}\right| \le \left|\frac{d_{ij}^{n0}}{d_{ij}^{n1}}\right|, \tag{13a}$$

$$r_{ij}^0 \le 1 \text{ and } r_{ij}^1 > 1 \text{ and } \left|\frac{r_{ij}^0 - 1}{r_{ij}^1 - 1}\right| \ge \left|\frac{d_{ij}^{n0}}{d_{ij}^{n1}}\right|, \tag{13b}$$

$$r_{ij}^0 \le 1 \text{ and } r_{ij}^1 \le 1. \tag{13c}$$

This trajectory tracking strategy is triggered by the conditions of $d_{ij}^{n0} > 0$ and $d_{ij}^{n1} < 0$. If the intersection point of segment $\boldsymbol{a}_i^0\boldsymbol{a}_i^1$ and line $\boldsymbol{b}_j\boldsymbol{b}_{j+1}$ is on the forward direction of $\boldsymbol{b}_j$ and backward direction of $\boldsymbol{b}_{j+1}$, the entrance position is in the region of contact cover $\boldsymbol{a}_i \sim \boldsymbol{b}_j\boldsymbol{b}_{j+1}$. The contact cover will be recognized as active.

In addition to the change of contact cover activity, the contact states may also change and the converged contact states is obtained through the OCI process. The judgment is based on the normal penetration distance and the relative tangential sliding distance of the locked points in a contact cover. The criteria to determine the contact states can be found in Ref. 14.

2.4 | Contact detection flowchart

In the analyzing procedure for discrete block system, the cover-based approach includes two parts: (1) establishment of the contact cover list and determination of activity and states of each contact cover at the beginning of each time step; and (2) adjustment of activity and states of contact cover after the solution of the equilibrium equation in OCI.

During the neighbor search phase, a list of neighbor block pairs is established. The cover-based search phase aims to find detailed geometrical data of two neighbor blocks, which belongs to the delicate search phase. A flowchart of the cover-based detection process at step beginning is shown in Figure 10. It contains two loops, the vertex-edge examination loop and the edge-vertex examination loop. A small portion of vertex-edge combinations will be added to C^L in above two loops. Then, the contact covers corresponding to distance d_{RE2} will be selected as active contact covers. The initial states of these active contact covers are determined by associated criteria in Section 2.3.

The flowchart of a vertex-edge examination loop is shown in Figure 11. In each examination loop, the entrance filter criterion and the distance filter criterion are used sequentially to select the valid vertex-edge pair. The vertex-edge pairs passing both criteria form valid contact covers and they are added to C^L.

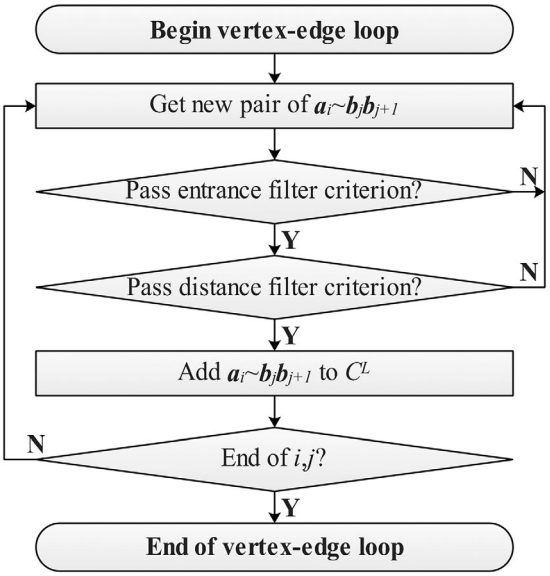

FIGURE 11 The flowchart of the vertex-edge examination loop

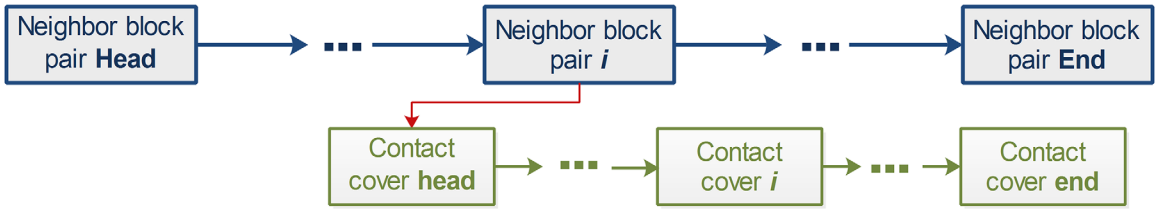

FIGURE 12 The data structure of the contact list in cover-based approach

2.5 | Contact data structure in program

In cover-based contact solution approach, the data structure is simple and clear. Each block in the system maintains a list of neighbor block pair. Each neighbor block pair maintains a contact cover list. Each contact cover contains a vertex-edge pair and flags indicating the activity and states, as shown in Figure 12.

2.6 | Adoption of tolerance values

During the contact analysis with the proposed approach, the entrance filter distance and the overlapping angle tolerance should be specified. To capture all potential contact covers, the contact tolerance d_n^{tol} should be at least twice larger than the maximum displacement d_{max} in a time step. The overlapping angle tolerance θ_e^{tol} should be at least twice the value of the maximum rotation angle θ_{max} in a time step. Meanwhile, the smallest angle of two edges should also be larger than the overlapping angle tolerance.

3 | FORMULATION AND ANALYSIS PROCEDURE OF DDA

In this paper, the cover-based contact detection approach is implemented in DDA. DDA is a discontinuous computation method featured by its implicit solution approach and OCI strategy to reach contact convergence.[14] The formulation of DDA and its typical analysis flow chart are briefly reviewed in this section.

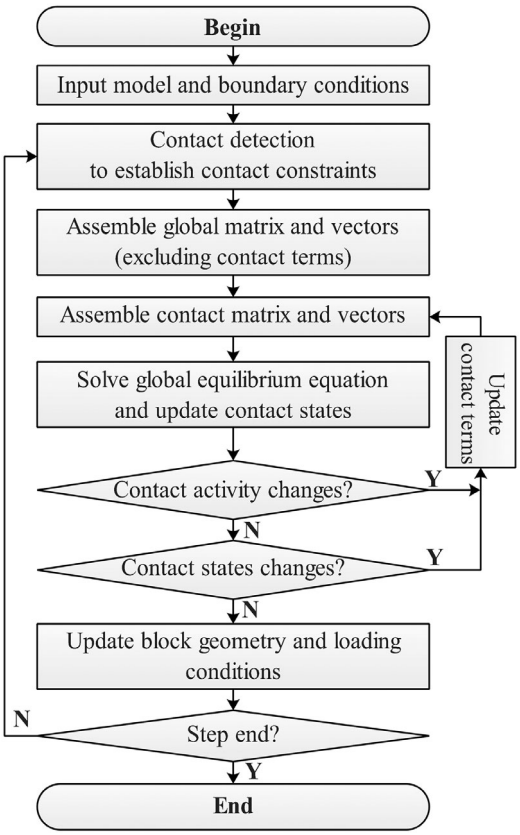

FIGURE 13 The flowchart of the implicit contact computation process

3.1 | Formulation of DDA

Each block is assumed to be linearly deformed with a constant strain distribution, as defined in Ref. 14. For both kinetic and static simulation of the displacement and deformation of a block system, a stepwise time integration strategy is applied. With the constant acceleration integration approach,[70,71] the equation of motion can be solved in the following way in each step:

$$\begin{bmatrix} \mathbf{K}_{11} & \mathbf{K}_{12} & \mathbf{K}_{13} & \cdots & \mathbf{K}_{1n} \\ \mathbf{K}_{21} & \mathbf{K}_{22} & \mathbf{K}_{23} & \cdots & \mathbf{K}_{2n} \\ \mathbf{K}_{31} & \mathbf{K}_{32} & \mathbf{K}_{33} & \cdots & \mathbf{K}_{3n} \\ \vdots & \vdots & \vdots & \ddots & \vdots \\ \mathbf{K}_{\mathrm{n}1} & \mathbf{K}_{\mathrm{n}2} & \mathbf{K}_{\mathrm{n}3} & \cdots & \mathbf{K}_{nn} \end{bmatrix} \begin{Bmatrix} \Delta \boldsymbol{d}_1 \\ \Delta \boldsymbol{d}_2 \\ \Delta \boldsymbol{d}_3 \\ \vdots \\ \Delta \boldsymbol{d}_n \end{Bmatrix} = \begin{Bmatrix} \boldsymbol{f}_1 \\ \boldsymbol{f}_2 \\ \boldsymbol{f}_3 \\ \vdots \\ \boldsymbol{f}_n \end{Bmatrix}, \tag{14}$$

where $\mathbf{K}_{ii}$ represents a 6×6 submatrix for block i; $\mathbf{K}_{ij}(i \neq j)$ represents a 6×6 contact submatrix with respect to block i and j; $\triangle \boldsymbol{d}_i$ represents the incremental degree of freedom values of block i; and $\boldsymbol{f}_i$ represents the force vectors acting on block i.

The penalty function approach is used to enforce the contact constraint. In each step, the geometrical information of all contact covers can be established through the proposed cover-based detection algorithm. With the known geometrical configurations of each contact cover $E(\boldsymbol{a}_i, \boldsymbol{b}_j \boldsymbol{b}_{j+1})$ or $E(\boldsymbol{a}_i \boldsymbol{a}_{i+1}, \boldsymbol{b}_j)$, the formulation of contact into Equation (14) can follow the work in Ref. 14.

3.2 | Procedure of DDA

The analysis procedure of DDA program as introduced by Shi[14] and many others[23,72] is replicated in Figure 13 considering the modifications of the cover-based approach. The stepwise analysis process is controlled by time steps. In each step,

TABLE 1 Key parameters of the simulation examples in Sections 4.1-4.3

Parameters	Unit	4.1	4.2	4.3(a)	4.3(b)
Max displacement	m	0.02	0.07	0.1	0.005
Max rotation	°	2	2	2	2
Contact tolerance	m	0.04	0.14	0.2	0.01
Initial time step size	s	0.01	0.01	0.01	0.002
Normal penalty	N/m	3×10^{10}	3×10^{10}	3×10^{10}	3×10^{10}

TABLE 2 Key parameters of the simulation cases in Section 4.4

Parameters	Unit	Case a	Case b	Case c
Max displacement	m	0.1	0.005	0.005
Max rotation	°	2	2	2
Contact tolerance	m	0.2	0.01	0.01
Initial time step size	s	0.01	0.0005	0.005
Normal penalty	N/m	3×10^{10}	3×10^{10}	3×10^{6}

contact detection is proceeded first to establish the contact constraints. Then, the matrix and vector terms in the global equilibrium equation are assembled. The equation is solved and contact activity and states of each contact cover will be checked by the proposed criteria. If change of activity or states occurs, associated contact terms will be updated and again the updated equilibrium equation will be solved. If the activity and states of all contact covers are converged, the block geometry and loading conditions will be updated. This stepwise solution process will be cycled until accumulated steps reach its maximum.

4 | ROBUSTNESS TESTS FOR IRREGULAR POLYGONS

The feasibility and robustness of the proposed cover-based approach in solving contact of irregular convex polygons during collisions are verified by several examples in this section. The proposed cover-based contact detection (CB-CD) approach and the conventional contact type-based contact detection strategies with the contact territory definition shown in Figure 1 (TB-CD-1) and Figure 2 (TB-CD-2) are used for comparisons. The robustness of all approaches in handling contacts of irregular polygons with large contact tolerance or small contact penalty values is tested in the following examples. In all examples belonging to this section, the following physical parameters for blocks are used: density $\rho = 2000\ \text{kg/m}^3$; elastic modulus $E = 1$ GPa; Poisson's ratio $\mu = 0.25$. Gravity is omitted and contact is assumed to be frictionless. Table 1 shows the contact parameters in examples 4.1, 4.2, and 4.3. Table 2 shows the contact parameters in example 4.4.

4.1 | Contact of sharp corners

This example investigates the robustness of various contact detection strategies in contact scenarios of triangles with sharp corners. Two triangles with small angles of 11.4° are generated, as shown in Figure 14A. Triangle A has an initial velocity of 1 m/s toward –y direction, and triangle B is fixed. The contact detection methods TB-CD-1, TB-CD-2, and CB-CD are applied in this collision simulation. The key parameters, which include the maximum step displacement, the contact tolerance, the maximum step rotation, the normal penalty parameters, and the initial time step size, are listed in Table 1.

The simulation results are shown in Figure 14B-D. Wrong contact pairs are detected by TB-CD-1 with the applied simulation parameters and the movement of triangle A after collision is not correct. By comparison, TB-CD-2 and CB-CD produce physically viable collision results.

4.2 | Contact of polygons with short edges

Voronoi polygons are commonly used in many simulations to investigate the grain structural effects of rock materials.[73,74] This example investigates the contact scenarios of two polygons which contains short edges. Two polygons with 18 edges

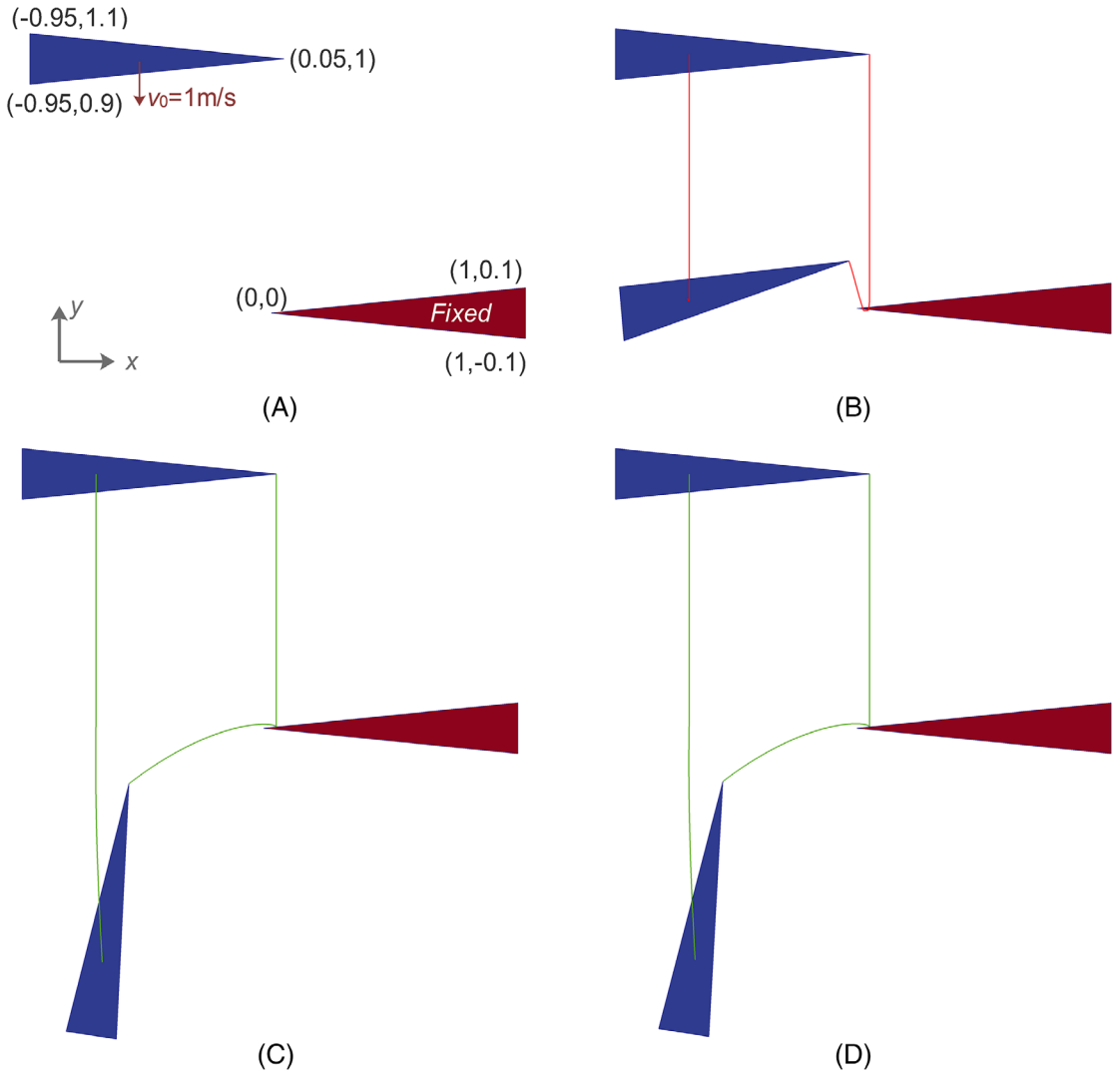

FIGURE 14 Contact simulation examples of two triangles with small angles: (A) the initial model; (B) the result by TB-CD-1 approach; (C) the result by TB-CD-2 approach; and (D) the result by CB-CD approach

are generated with the edge length of 0.35 m, and are shown in Figure 15A. In all three cases, polygon A has an initial velocity of 5 m/s along –y direction, while all vertices of polygon B are fixed. The key parameters in these simulation cases are listed in Table 1. Figure 15B-D shows the movement trajectory of polygon A. With the applied parameters, wrong contact pairs are detected by TB-CD-2 strategy and the movement trend of particle A after collision is not correct. By comparison, the simulation results by TB-CD-1 and CB-CD strategies are physically permissible.

4.3 | Contact of flat polygons with small edges

This example investigates the contact scenarios of flat polygons with small edges. The geometrical configuration of the two flat polygons is shown in Figure 16A, where the minimum edge is 0.02 m. Block A has an initial velocity of 1 m/s and block B is fixed. In this example, cases (a) and (b) with different maximum displacements and different contact tolerances are used by TB-CD-1, TB-CD-2, and CB-CD approaches. All key simulation parameters are listed in Table 1.

The simulation results of the collision process for case *a* and case *b* are shown in Figure 16B-G. When large contact tolerance (0.2 m) is used, wrong contact pairs are detected by TB-CD-1 and TB-CD-2 approaches and the moving trajectories of block A after collision are not correct. When small contact tolerance (0.01 m) is used, the results by TB-CD-1

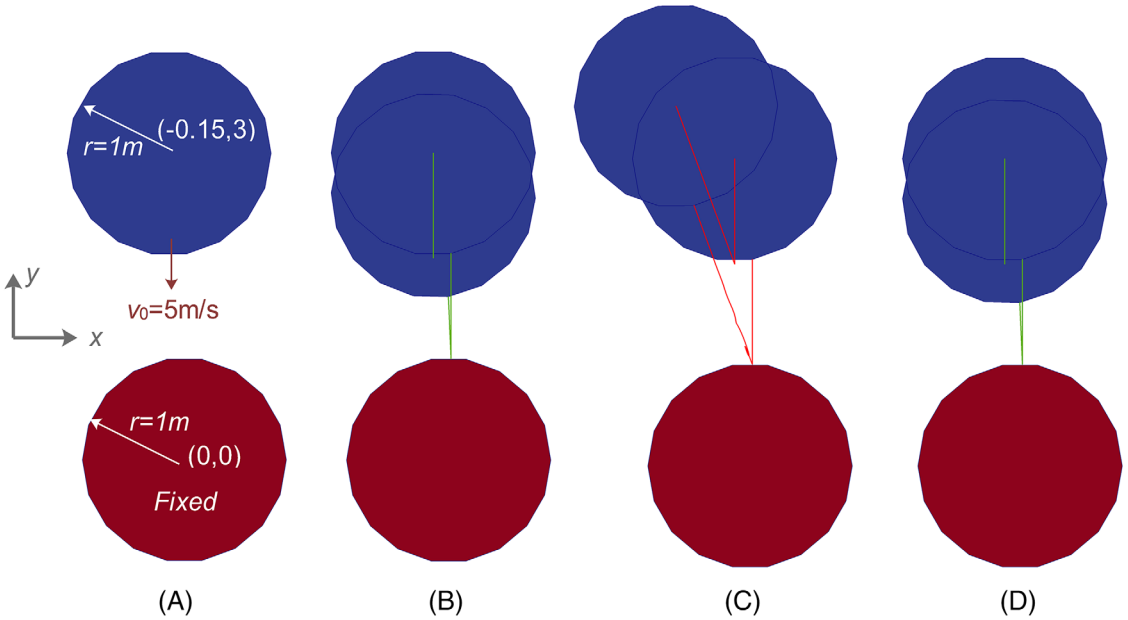

FIGURE 15 Contact simulation examples of two polygons with many small edges: (A) the initial model; (B) the result by TB-CD-1 approach; (C) the result by TB-CD-2 approach; and (D) the result by CB-CD approach

and TB-CD-2 approaches are physically permissible. Whenever large or small contact tolerances are used, the results by CB-CD approach are always correct.

4.4 | Contact of a corner and a small edge

This example investigates the robustness of the proposed algorithm in treating approaching vertex and small edge. Two blocks are generated, as shown in Figure 17A. Block A has a small edge with a length of 0.02 m and it has an initial velocity of 5 m/s along –y direction. Block B is fixed. In this example, cases (a), (b), and (c) with different contact tolerances and various contact penalty values are used to test the robustness of type-based and cover-based contact detection approaches. The key parameters in this example are shown in Table 2.

The simulation results for the three cases are shown in Figure 17B-J. When large contact tolerance (0.2 m) and large penalty parameter (3×10^{10} N/m) are used, wrong contact pairs are detected by both TB-CD-1 and TB-CD-2 approaches, resulting in physically implausible results. When small contact tolerance (0.005 m) and large penalty parameter (3×10^{10} N/m) are used, the results by TB-CD-1 and TB-CD-2 approaches are correct. However, when small contact tolerance (0.005 m) and small penalty parameters (3×10^{6} N/m) are used, uncontrolled interpenetration occurs in the results by TB-CD-1 and TB-CD-2 approaches. When small penalty parameter (3×10^{6} N/m) is used, large contact tolerance (0.2 m) can be used by CB-CD approach without introducing incorrect contact covers, and the collision simulation result is correct. For all tested parameter combinations, the simulation results by CB-CD approach are correct.

4.5 | Discussions

In Section 4, four examples involving contact of irregular polygons are specially designed for robustness test of various contact detection approaches. The examples include contact scenarios of two sharp corners, two small edges, a corner and a small edge, and polygons with short edges. In above cases with extreme geometries, the conventional type-based detection approaches TB-CD-1 and TB-CD-2 may establish wrong contact types and produce unrealistic block collision results if the contact tolerance or contact penalty value is not carefully chosen. For example, TB-CD-1 approach and TB-CD-2 approach produce incorrect collision results when large contact tolerances are used in examples 4.1-4.3; TB-CD-1 approach and TB-CD-2 approach only produce the correct collision results when small contact tolerance and large penalty value are used. By

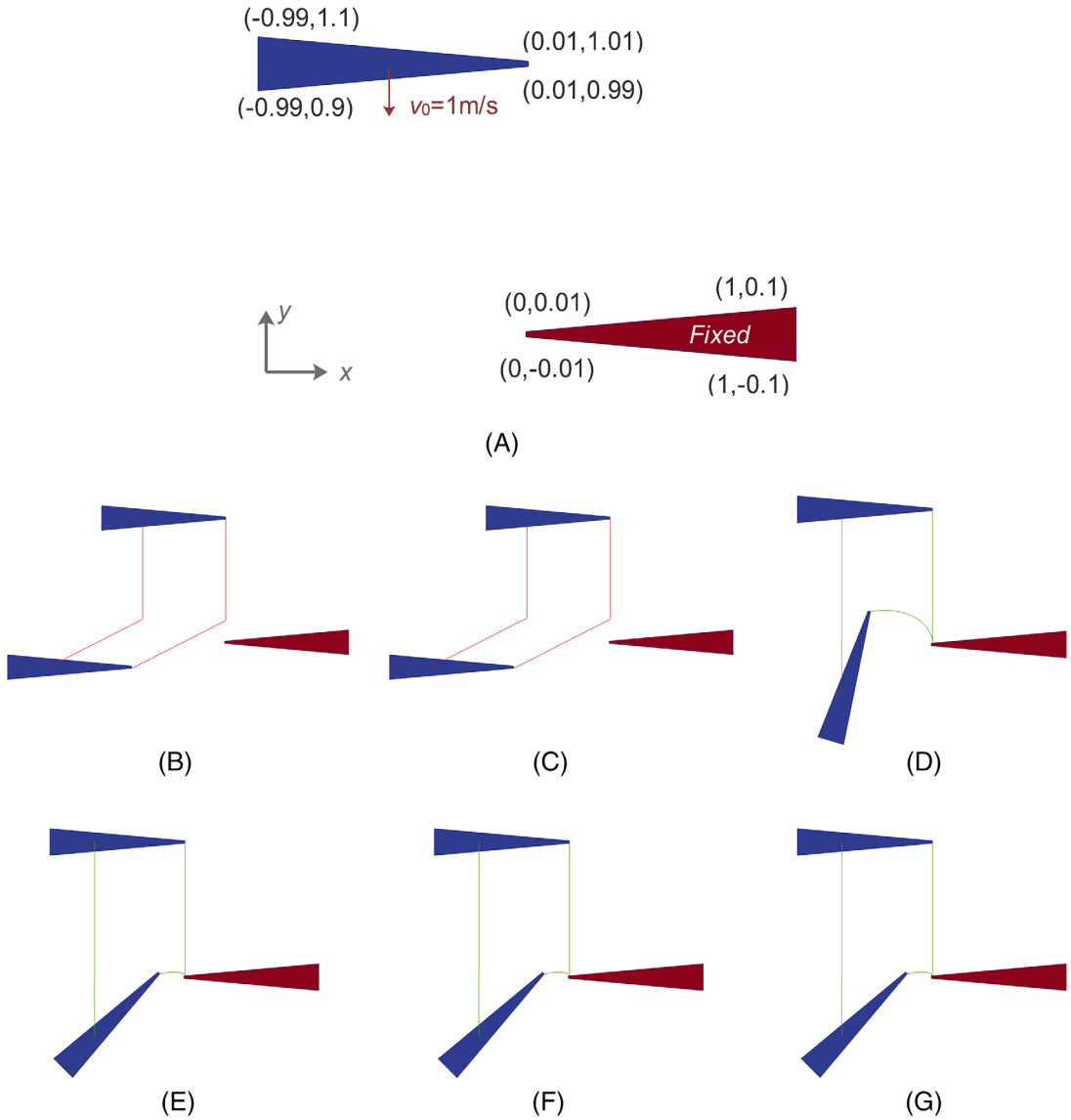

FIGURE 16 Contact simulation examples of two flat polygons with small edges: (A) the initial model; (B) the result by TB-CD-1 approach in case *a*; (C) the result by TB-CD-2 approach in case *a*; (D) the result by CB-CD approach in case *a*; (E) the result by TB-CD-1 approach in case *b*; (F) the result by TB-CD-2 approach in case *b*; and (G) the result by CB-CD approach in case *b*

comparison, the proposed cover-based detection approach always produces physically permissible results in all examples regardless of the usage of large contact tolerances or small penalty values.

5 | EFFICIENCY EVALUATIONS FOR BLOCK SYSTEM

The efficiency and robustness of the cover-based contact detection approach in kinetic analysis of polygonal block systems are tested in this section. In all simulation cases, a neighbor block search strategy based on the detection of axes-aligned bounding box concept is applied, as in original DDA approach.[75] For the delicate search phase, the type-based contact detection approach TB-CD-2 and the proposed cover-based contact detection approach CB-CD are applied. The efficiency improvement with different contact tolerances is evaluated and analyzed, considering blocks of various polygonal shapes and different block numbers. To keep the correctness of the simulation by TB-CD-2 approach, the basic contact tolerances are set to 0.2 multiplied by the minimum edge length. For the CB-CD approach, various contact tolerances are used, ranging from 1 to 10 times of the basic value used in TB-CD-2 approach.

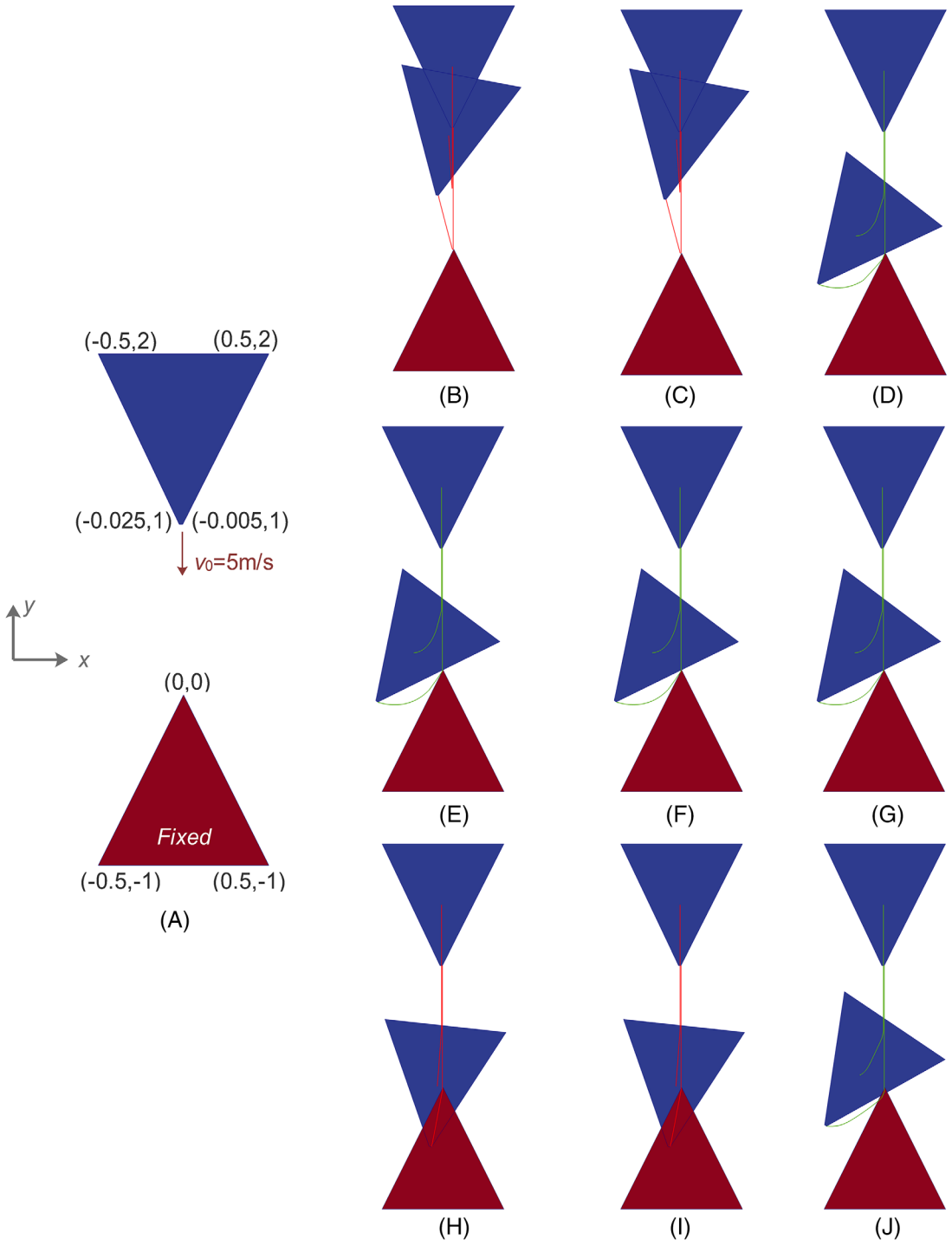

FIGURE 17 Contact simulation examples of approaching vertex and small edge: (A) the initial model; (B) the result by TB-CD-1 approach in case *a*; (C) the result by TB-CD-2 approach in case *a*; (D) the result by CB-CD approach in case *a*; (E) the result by TB-CD-1 approach in case *b*; (F) the result by TB-CD-2 approach in case *b*; (G) the result by CB-CD approach in case *b*; (H) the result by TB-CD-1 approach in case *c*; (I) the result by TB-CD-2 approach in case *c*; and (J) the result by CB-CD approach in case *c*

The computational steps, OCI cycles, and CPU cost for contact detection and examination are recorded for the efficiency evaluations. In this section, two dimensionless parameters, the contact tolerance ratio (r_{tol}) and contact detection speed-up ratio (r_{cd}), are defined. The contact tolerance ratio (r_{tol}) is

$$r_{tol} = \frac{d^{CB}}{d^{TB}}, \tag{15}$$

TABLE 3 The key parameters of the tested examples in Sections 5.1 and 5.2

Parameters	Unit	5.1(a)	5.1(b)	5.2(a)	5.2(b)
Block number		20	93	229	826
Min edge length	m	0.243	0.2	0.135	0.13
Max displacement	m	0.0243	0.02	0.0135	0.013
Max rotation	°	2	2	2	2
Contact tolerance	m	0.0487	0.04	0.027	0.026
Initial time step size	s	0.05	0.02	0.02	0.005
Normal penalty	N/m	3×10^{10}	3×10^{10}	3×10^{9}	3×10^{9}
Analysis time	s	1.0	1.0	1.0	1.0

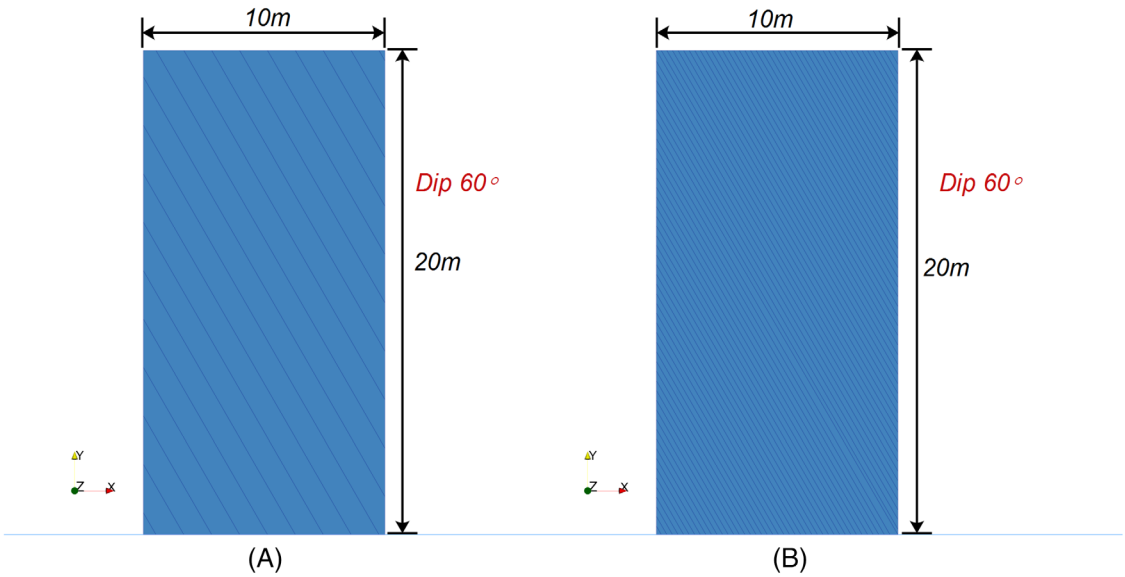

FIGURE 18 The column models cut by one joint set: (A) model 1 with 20 blocks; and (B) model 2 with 93 blocks

where d^{CB} and d^{TB} are the contact tolerances used in CB-CD and TB-CD-2 approaches, respectively. The contact detection speed-up ratio (r_{cd}) is

$$r_{cd} = \frac{T^{TB}}{T^{CB}}, \tag{16}$$

where T^{TB} and T^{CB} are the CPU cost in contact detection and judgment processes by TB-CD-2 and CB-CD approaches, respectively.

For all simulated examples in this section, the physical parameters for blocks are as follows: density $\rho = 2600$ kg/m^3; elastic modulus $E = 1$ GPa; Poisson's ratio $\mu = 0.3$; gravity acceleration $g = 9.8$ m/s^2. The contact parameters are listed in Table 3.

5.1 | Failure of a column cut by one joint set

In this example, a column with the size of 10 m × 20 m is cut by a joint set with dip angle of 60°. The potential failure of this joint column under gravity effect on a frictionless surface is analyzed. Two models are generated, considering different joint spacing values, as shown in Figure 18. Model (a) consists of 20 blocks with a minimum block edge of 0.243 m. Model (b) consists of 93 blocks with a minimum block edge of 0.2 m. To capture the potential failure process, the joints are assumed frictionless. A total analysis period is 1.0 s and the key parameters in the simulation are listed in Table 3.

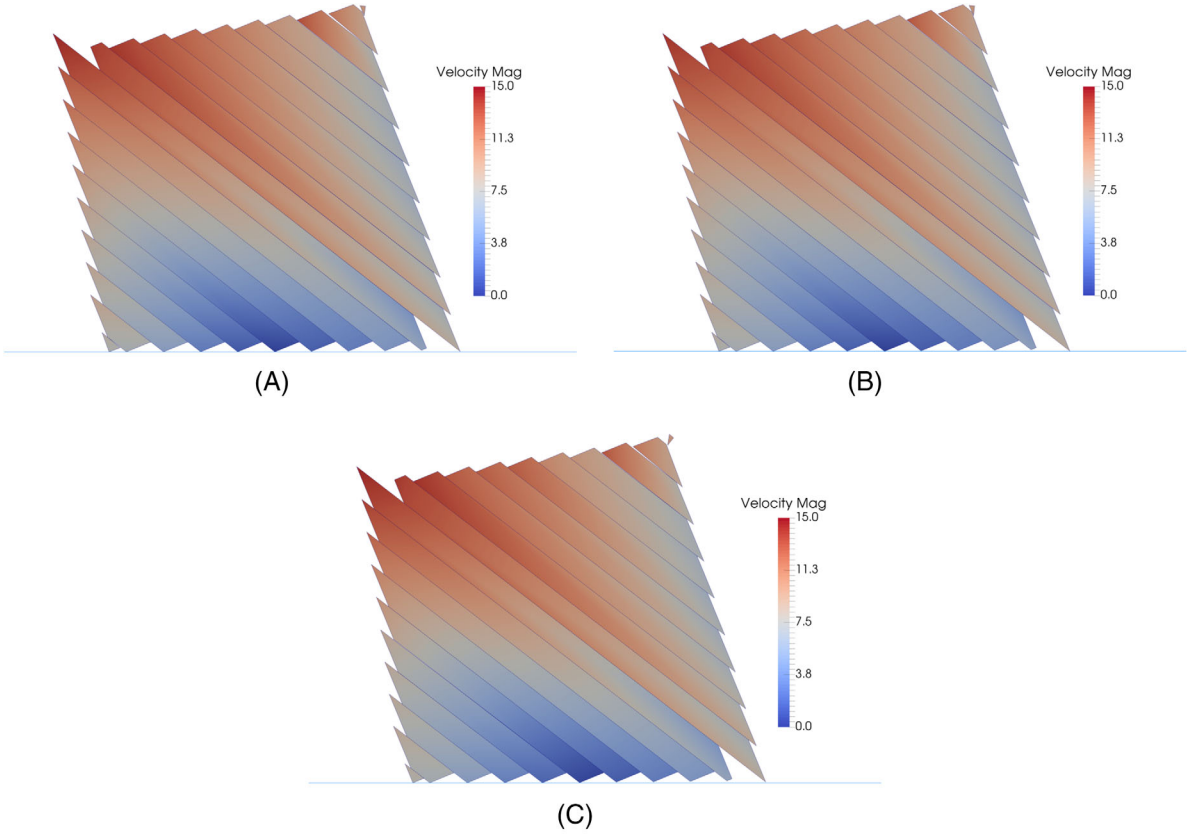

FIGURE 19 The block system after 1.0 s for model (a) in Section 5.1: (A) the result by TB-CD-2 approach; (B) the result by CB-CD approach with $r_{tol} = 1$; and (C) the result by TB-CD-2 approach with $r_{tol} = 10$

The configurations of the block systems after 1.0 s for model (a) and model (b) by various approaches are shown in Figures 19 and 20. The total computational steps, the total OCI cycles, and the CPU cost for contact detection during the 1.0 s simulation are listed in Table 4. The results by TB-CD-2 and CB-CD approaches with different contact tolerances are very similar. Note that the step size is changed automatically to meet the maximum displacement and OCI convergence requirement. Different step sizes may be used for simulation with different r_{tol} values. As the numerical damping effect in DDA is closely related to time step,[70,71] the simulation results can be slightly different with various r_{tol}. The contact detection speed-up ratio with different contact tolerance ratios is shown in Figure 21. For case (a) with 20 blocks, r_{cd} increases from 2 to 11 when r_{tol} increases from 1 to 10. For case (b) with 93 blocks, r_{cd} increases from 2 to 5 when r_{tol} increases from 1 to 4; r_{cd} then fluctuates from 5 to 6 when r_{tol} increases from 4 to 10.

5.2 | Failure of complex block system

In this example, a column with the size of 10 m × 20 m is cut by two joint sets with dip angles of 60° and 15°. Two models are generated, considering two different cases of joint spacing, as shown in Figure 22. Model (a) consists of 229 blocks, with a minimum edge of 0.135 m. Model (b) consists of 826 blocks, with a minimum edge of 0.13 m. The block system can slide along a horizontal surface under gravity. All contacts for blocks and the boundary line are assumed to be frictionless to track the potential failure process. A time period of 1.0 s is simulated and the parameters in all simulation cases are shown in Table 5.

The block systems for two models after 1.0 s by TB-CD-1 approach and CB-CD approach ($r_{tol} = 1$ and $r_{tol} = 10$) are shown in Figures 23 and 24. The total number of computational steps, the total number of OCI cycles, and the CPU cost for contact detection during the 1.0 s simulation are listed in Table 5. The two approaches with different parameters produce very similar results. Like the examples in Section 5.1, the numerical damping effects vary for simulations with various r_{tol}. This possibly results in slight differences of block configurations in Figures 23 and 24. The contact detection speed-up

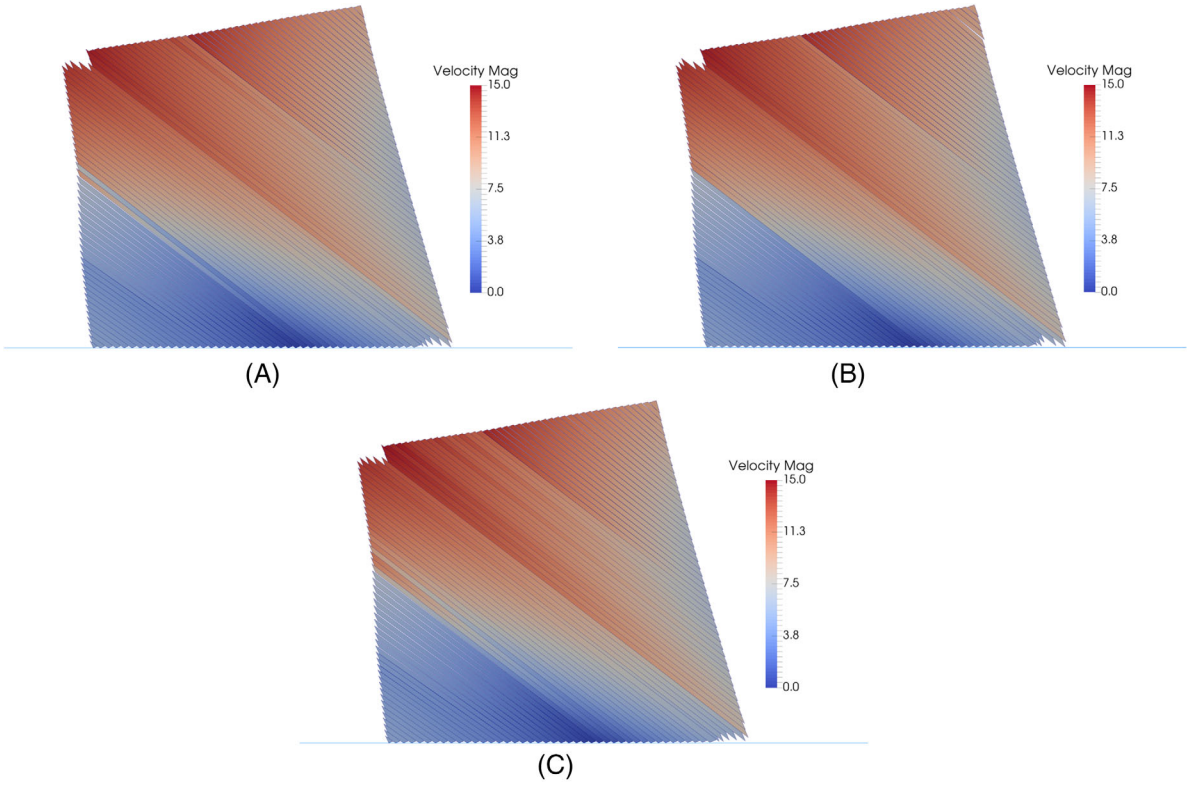

FIGURE 20 The block system after 1.0 s for model (b) in Section 5.1: (A) the result by TB-CD-2 approach; (B) the result by CB-CD approach with $r_{tol} = 1$; and (C) the result by TB-CD-2 approach with $r_{tol} = 10$

TABLE 4 The recording results of analysis step number and contact detection cost of the two cases in Section 5.1

Parameters	Unit	TB-CD-2	CB-CD $r_{tol} = 1$	CB-CD $r_{tol} = 2$	CB-CD $r_{tol} = 4$	CB-CD $r_{tol} = 6$	CB-CD $r_{tol} = 8$	CB-CD $r_{tol} = 10$
(a)Total steps	\	644	633	340	183	144	111	105
(a)OCI cycles	\	1325	1270	912	569	533	467	441
(a)CD cost	s	1.773	0.754	0.4284	0.2448	0.2081	0.1655	0.1577
(b)Total steps	\	774	789	427	274	259	220	222
(b)OCI cycles	\	2146	2375	1612	1235	1335	1173	1190
(b)CD cost	s	43.37	21.46	12.34	8.05	8.86	7.7	8.38

ratio with different contact tolerance ratios is shown in Figure 25. For the model with 229 blocks, r_{cd} is 1.5 when r_{tol} is 1; r_{cd} fluctuates around 2 when r_{tol} is from 2 to 10. For the model with 826 blocks, r_{cd} is around 1 when r_{tol} is 1 to 4; it then gradually reduces to 0.5 when r_{tol} increases from 4 to 10.

5.3 | Discussions

The robustness and efficiency of the proposed cover-based approach in solving contacts of complex polygonal block systems are two concerned points in Section 5. Its robustness is verified through the physically permissible block configurations obtained by simulations using the cover-based approach and type-based approach. The simulation results using different r_{tol} values show similar patterns in examples 5.1 and 5.2, and the differences in block configuration are associated with various numerical damping effects using the automatic time step control strategy. The examples also show that reliable results can be obtained by the cover-based approach when large contact tolerances are used.

For the computational efficiency, additional speed-up is obtained by increasing the contact tolerance ratio in most cases, as using larger contact tolerances tends to save more computational steps in reaching the targeting simulation time. Two

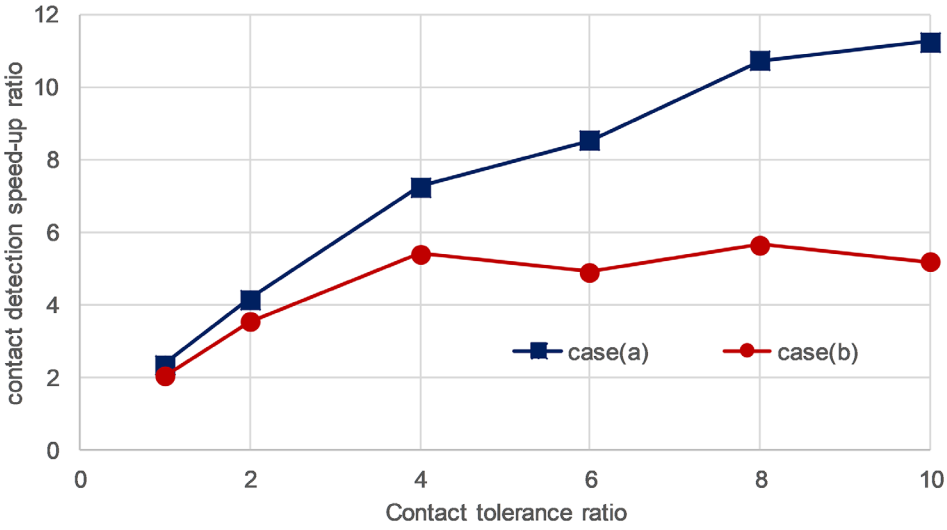

FIGURE 21 The speed-up ratio of CB-CD approach when different contact tolerance ratio is adopted in example 5.1

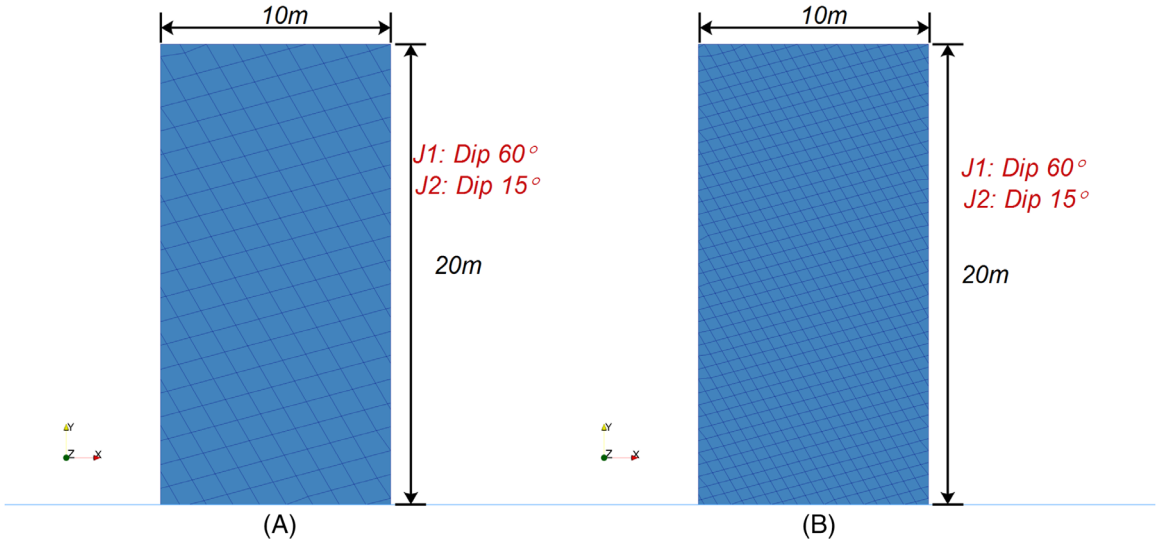

FIGURE 22 The column models cut by two joint sets: (A) model 1 with 229 blocks; and (B) model 2 with 826 blocks

phenomena are observed through the two simulation examples: (1) A contact detection speed-up ratio between 1 and 2.2 is obtained when the same contact tolerances are used by CB-CD approach and TB-CD-2 approach, illustrating that the proposed CB-CD approach outperforms the TB-CD-2 approach; (2) More significant speed-up effects are observed for block system with simple geometries when larger contact tolerance ratio is used. When same contact tolerance ratios are used, the speed-up ratio decreases with increasing block numbers and increasing complexities of block geometries, which is due to the increasing computational steps or the overhead of detecting more contact covers in reaching the targeting simulation time.

6 | CONCLUSIONS

Contact interaction of multiple body system with polygonal shapes is a typical scenario in many geotechnical engineering problems and the irregular polygonal shapes with extreme geometries (eg, sharp corners and small edges) pose a challenge to the robustness of conventional contact detection algorithms. The simulation examples in Section 4 show the conventional type-based contact detection approach may produce incorrect results if the contact tolerance or the contact penalty is not appropriately chosen.

TABLE 5 The recording results of analysis step number and contact detection cost of the two cases in Section 5.2

Parameters	Unit	TB-CD-2	CB-CD $r_{tol} = 1$	CB-CD $r_{tol} = 2$	CB-CD $r_{tol} = 4$	CB-CD $r_{tol} = 6$	CB-CD $r_{tol} = 8$	CB-CD $r_{tol} = 10$
(a)Total steps	\	1111	1138	628	433	446	447	426
(a)OCI cycles	\	3324	3485	2425	2105	2045	2242	2073
(a)CD cost	s	21.25	15.56	10.48	9.68	10.13	11.64	12.06
(b)Total steps	\	1227	1333	1001	965	981	1004	971
(b)OCI cycles	\	5226	6051	5690	5811	5883	6030	5783
(b)CD cost	s	111.3	107.3	106.1	108.4	144.6	172.3	191.49

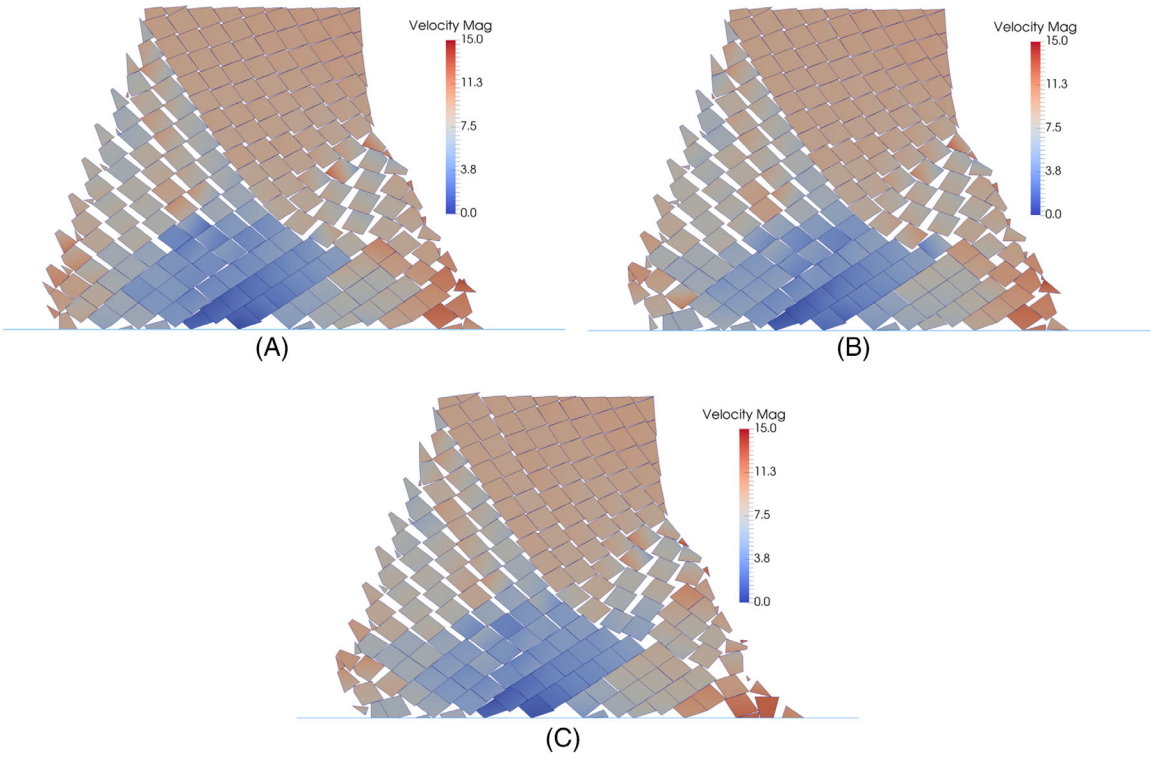

FIGURE 23 The block system after 1.0 s for model (a) in Section 5.2: (A) the result by TB-CD-2 approach; (B) the result by CB-CD approach with $r_{tol} = 1$; and (C) the result by TB-CD-2 approach with $r_{tol} = 10$

Focusing on the robustness and efficiency issues in treating irregular convex polygons, this paper proposes a cover-based approach to detect and solve the contact constraints for convex polygons. The major theoretical improvement is the application of global detection and determination of contact covers instead of the conventional contact type-based local detection strategies. With the proposed cover-based approach, a simple contact data structure is maintained in analysis. Each polygon maintains a neighbor block list, where each neighbor block pair maintains a contact cover list with contact information of vertex-edge pairs. The entrance filter criterion and distance filter criterion are used to establish the contact cover list in each step. Only the active contact covers determined globally by the distance rule in Equation (11) or trajectory-tracking strategy in Equations (12) and (13) are used for contact formulation. In OCI, the activity and states of each contact cover are updated. Compared to conventional type-based approach, the major advantages of the proposed cover-based approach in terms of robustness and efficiency are as follows:

1. It provides a more robust solution for contact analysis of irregular polygons with small angles or small edges. This is verified by examples in Sections 4 and 5. Due to the global detection of all potential contact covers and the global determination of the activity and states of each contact cover, it always provides physically permissible results regardless of the applied contact tolerances or contact penalty values. By comparison, the conventional type-based detection approach may lead to incorrect results with inappropriate contact parameters.

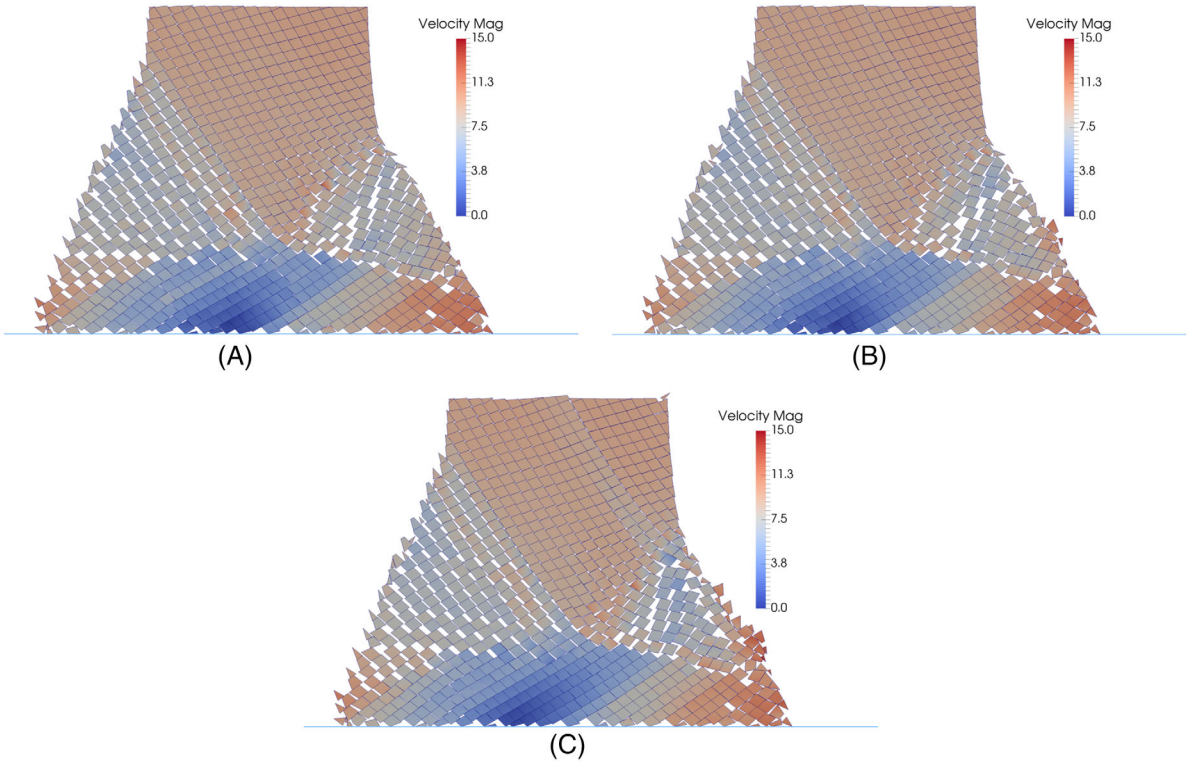

FIGURE 24 The block system after 1.0 s for model (b) in Section 5.2: (A) the result by TB-CD-2 approach; (B) the result by CB-CD approach with $r_{tol} = 1$; and (C) the result by TB-CD-2 approach with $r_{tol} = 10$

FIGURE 25 The speed-up ratio of CB-CD approach when different contact tolerance ratio is adopted in example 5.2

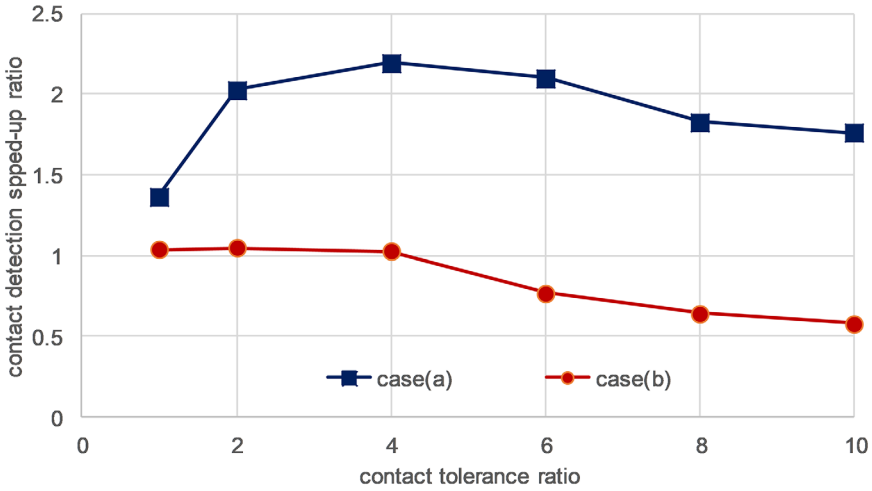

2. It facilitates more efficient contact detection for convex polygons. This is verified by examples in Section 5. First, it outperforms the TB-CD-2 approach when the same contact tolerances are used; second, larger speed-up ratios can be obtained with larger contact tolerance ratios in the simulation examples. However, it should be noted that very large contact tolerance should also be avoided for block system with complex geometries and large number of blocks due to the potential overhead of checking more contact covers.

Some possible extensions of the proposed approach are worth to mention. First, the method can be easily extended to explicit solution schemes. Second, it can be extended to be applicable to concave polygons by decomposing the concave blocks into a subset of convex blocks. Third, the idea of cover-based approach can be used for more robust and efficient analysis of irregular 3D polyhedral blocks.

ACKNOWLEDGMENTS

This study was financially supported by Sofja Kovalevskaja Program from Alexander von Humboldt Foundation and the National Natural Science Foundation of China (51479191 and 11672360).

Open access funding enabled and organized by Projekt DEAL.

ORCID

Xiaoying Zhuang https://orcid.org/0000-0001-6562-2618
Fei Zheng https://orcid.org/0000-0003-2321-9112
Hong Zheng https://orcid.org/0000-0002-8108-3009
Yu-Yong Jiao https://orcid.org/0000-0001-9081-6932

REFERENCES

1. Wriggers P, Zavarise G. Computational contact mechanics. *Encyclopedia of* Computational Mechanics. 2004.
2. Munjiza AA, Knight EE, Rougier E. *Computational Mechanics of Discontinua*. John Wiley & Sons; 2011.
3. Jing L, Stephansson O. *Fundamentals of Discrete Element Methods for Rock Engineering: Theory and Applications*. Elsevier; 2007.
4. Zheng F, Zhuang X, Zheng H, Jiao Y-Y, Rabczuk T. Kinetic analysis of polyhedral block system using an improved potential-based penalty function approach for explicit discontinuous deformation analysis. *Appl Math Modell*. 2020;82:314–335.
5. Wu J-H, Chen C-H. Application of DDA to simulate characteristics of the Tsaoling landslide. *Comput Geotech*. 2011;38(5):741–750.
6. Wu W, Zhu H, Lin J-S, Zhuang X, Ma G. Tunnel stability assessment by 3D DDA-key block analysis. *Tunnel Undergr Space Technol*. 2018;71:210–214.
7. Liu G, Li J, Kang F. Failure mechanisms of toppling rock slopes using a three-dimensional discontinuous deformation analysis method. *Rock Mech Rock Eng*. 2019;52(10):3825–3848.
8. Peng X, Yu P, Zhang Y, Chen G. Applying modified discontinuous deformation analysis to assess the dynamic response of sites containing discontinuities. *Eng Geol*. 2018;246:349–360.
9. Gardner M, Sitar N. Modeling of dynamic rock–fluid interaction using coupled 3-D discrete element and lattice Boltzmann methods. *Rock Mech Rock Eng*. 2019;52(12):5161–5180.
10. Goodman RE, Taylor RL, Brekke TL. A model for the mechanics of jointed rock. *J Soil Mech Found Div*. 1968;94(3):637–659.
11. Zhou S, Rabczuk T, Zhuang X. Phase field modeling of quasi-static and dynamic crack propagation: COMSOL implementation and case studies. *Adv Eng Softw*. 2018;122:31–49.
12. Ren H, Zhuang X, Cai Y, Rabczuk T. Dual-horizon peridynamics. *Int J Numer Methods Eng*. 2016;108(12):1451–1476.
13. Cundall PA, Strack OD. A discrete numerical model for granular assemblies. *Geotechnique*. 1979;29(1):47–65.
14. Shi G-H. *Discontinuous Deformation Analysis—A New Numerical Model for the Static and Dynamics of Block System*. University of California, Berkeley; 1988.
15. Do TN, Wu J-H. Simulation of the inclined jointed rock mass behaviors in a mountain tunnel excavation using DDA. *Comput Geotech*. 2020;117:103249.
16. Zhao GF, Fang J, Zhao J. A 3D distinct lattice spring model for elasticity and dynamic failure. *Int J Numer Anal Methods Geomech*. 2011;35(8):859–885.
17. Yao C, Jiang Q, Shao J-F. Numerical simulation of damage and failure in brittle rocks using a modified rigid block spring method. *Comput Geotech*. 2015;64:48–60.
18. Munjiza AA. *The Combined Finite-Discrete Element Method*. John Wiley & Sons; 2004. https://onlinelibrary.wiley.com/doi/book/10.1002/0470020180.
19. Ma G, An X, Zhang H, Li L. Modeling complex crack problems using the numerical manifold method. *Int J Fract*. 2009;156(1):21–35.
20. Li X, Zhao J. An overview of particle-based numerical manifold method and its application to dynamic rock fracturing. *J Rock Mech Geotech Eng*. 2019;11:684–700.
21. He L, An X, Ma G, Zhao Z. Development of three-dimensional numerical manifold method for jointed rock slope stability analysis. *Int J Rock Mech Min Sci*. 2013;64:22–35.
22. Wang X, Wu W, Zhu H, Lin J-S, Zhang H. Contact detection between polygonal blocks based on a novel multi-cover system for discontinuous deformation analysis. *Comput Geotech*. 2019;111:56–65.
23. Wu W, Zhu H, Zhuang X, Ma G, Cai Y. A multi-shell cover algorithm for contact detection in the three dimensional discontinuous deformation analysis. *Theor Appl Fract Mech*. 2014;72:136–149.
24. Zhang H, Chen G, Zheng L, et al. Detection of contacts between three-dimensional polyhedral blocks for discontinuous deformation analysis. *Int J Rock Mech Min Sci*. 2015;78:57–73.
25. Zheng F, Jiao Y, Leung YF, Zhu J. Algorithmic robustness for contact analysis of polyhedral blocks in discontinuous deformation analysis framework. *Comput Geotech*. 2018;104:288–301.
26. Zheng F, Jiao Y-Y, Zhang X-L, Tan F, Wang L, Zhao Q. Object-oriented contact detection approach for three-dimensional discontinuous deformation analysis based on entrance block theory. *Int J Geomech*. 2016;17(5):E4016009.

27. Cundall PA. Formulation of a three-dimensional distinct element model—Part I. A scheme to detect and represent contacts in a system composed of many polyhedral blocks. *Int J Rock Mech Min Sci Geomech Abstracts*. 1988;25(3):107–116.
28. Fu X, Sheng Q, Zhang Y, Chen J. Investigation of highly efficient algorithms for solving linear equations in the discontinuous deformation analysis method. *Int J Numer Anal Methods Geomech*. 2016;40(4):469–486.
29. Huang GH, Xu YZ, Yi XW, Xia M, Jiao YY, Zhang S. Highly efficient iterative methods for solving linear equations of three-dimensional sphere discontinuous deformation analysis. *Int J Numer Anal Methods Geomech*. 2020;44:1301–1314.
30. Huang G-H, Xu Y-Z, Chen X-F, Xia M, Zhang S, Yi X-W. A new C++ programming strategy for three-dimensional sphere discontinuous deformation analysis. *Int J Geomech*. 2020;20(10):04020175.
31. Munjiza A, Andrews K. NBS contact detection algorithm for bodies of similar size. *Int J Numer Methods Eng*. 1998;43(1):131–149.
32. Perkins E, Williams JR. A fast contact detection algorithm insensitive to object sizes. *Eng Comput*. 2001;18(1/2):48–62.
33. Williams JR, Perkins E, Cook B. A contact algorithm for partitioning N arbitrary sized objects. *Eng Comput*. 2004;21(2/3/4):235–248.
34. Zheng Y, Xia L, Yu Q. Identifying rock blocks based on exact arithmetic. *Int J Rock Mech Min Sci*. 2016;86:80–90.
35. Lei Q, Latham J-P, Tsang C-F. The use of discrete fracture networks for modelling coupled geomechanical and hydrological behaviour of fractured rocks. *Comput Geotech*. 2017;85:151–176.
36. Abdelaziz A, Zhao Q, Grasselli G. Grain based modelling of rocks using the combined finite-discrete element method. *Comput Geotech*. 2018;103:73–81.
37. Li X, Li H, Zhao J. The role of transgranular capability in grain-based modelling of crystalline rocks. *Comput Geotech*. 2019;110:161–183.
38. Lin CT, Amadei B, Jung J, Dwyer J. Extensions of discontinuous deformation analysis for jointed rock masses. *Int J Rock Mech Min Sci Geomech Abstracts*. 1996;33(7):671–694.
39. Rougier E, Munjiza A, John N. Numerical comparison of some explicit time integration schemes used in DEM, FEM/DEM and molecular dynamics. *Int J Numer Methods Eng*. 2004;61(6):856–879.
40. Zheng F, Leung YF, Zhu JB, Jiao YY. Modified predictor-corrector solution approach for efficient discontinuous deformation analysis of jointed rock masses. *Int J Numer Anal Methods Geomech*. 2019;43(2):599–624.
41. Zheng H, Li X. Mixed linear complementarity formulation of discontinuous deformation analysis. *Int J Rock Mech Min Sci*. 2015;75:23–32.
42. Zheng H, Zhang P, Du X. Dual form of discontinuous deformation analysis. *Comput Meth Appl Mech Eng*. 2016;305:196–216.
43. Peng X, Yu P, Chen G, Xia M, Zhang Y. CPU-accelerated explicit discontinuous deformation analysis and its application to landslide analysis. *Appl Math Modell*. 2020;77:216–234.
44. Fan H, Wang J, Zheng H. Variational inequality-based particle discontinuous deformation analysis. *Int J Numer Anal Methods Geomech*. 2019;43(11):1995–2019.
45. Meng J, Cao P, Huang J, Lin H, Li K, Cao R. Three-dimensional spherical discontinuous deformation analysis using second-order cone programming. *Comput Geotech*. 2019;112:319–328.
46. Yang Y, Xu D, Zheng H. Explicit discontinuous deformation analysis method with lumped mass matrix for highly discrete block system. *Int J Geomech*. 2018;18(9):04018098.
47. Jiang Q, Yeung M. A model of point-to-face contact for three-dimensional discontinuous deformation analysis. *Rock Mech Rock Eng*. 2004;37(2):95–116.
48. Zhang H, Liu S-G, Zheng L, et al. Extensions of edge-to-edge contact model in three-dimensional discontinuous deformation analysis for friction analysis. *Comput Geotech*. 2016;71:261–275.
49. Ni K, Ning Y, Yang J, Chen Z. Contact detection by the contact theory in 2D-DDA for arbitrary polygonal blocks. *Eng Anal Boundary Elem*. 2020;119:203–213.
50. Zheng F, Jiao YY, Sitar N. Generalized contact model for polyhedra in three-dimensional discontinuous deformation analysis. *Int J Numer Anal Methods Geomech*. 2018;42(13):1471–1492.
51. Zheng F, Jiao Y-Y, Gardner M, Sitar N. A fast direct search algorithm for contact detection of convex polygonal or polyhedral particles. *Comput Geotech*. 2017;87:76–85.
52. Itasca U. *Version 4.0 User's Manuals*. Minneapolis, MN: Itasca Consulting Group; 2004.
53. Wu W, Wang X, Zhu H, Shou K-J, Lin J-S, Zhang H. Improvements in DDA program for rockslides with local in-circle contact method and modified open-close iteration. *Eng Geol*. 2020;265:105433.
54. Houlsby G. Potential particles: a method for modelling non-circular particles in DEM. *Comput Geotech*. 2009;36(6):953–959.
55. Boon C, Houlsby G, Utili S. A new algorithm for contact detection between convex polygonal and polyhedral particles in the discrete element method. *Comput Geotech*. 2012;44:73–82.
56. Feng Y, Han K, Owen D. Energy-conserving contact interaction models for arbitrarily shaped discrete elements. *Comput Meth Appl Mech Eng*. 2012;205-208:169–177.
57. Munjiza A, Andrews K. Penalty function method for combined finite–discrete element systems comprising large number of separate bodies. *Int J Numer Methods Eng*. 2000;49(11):1377–1396.
58. Yan C, Zheng H. A new potential function for the calculation of contact forces in the combined finite–discrete element method. *Int J Numer Anal Methods Geomech*. 2017;41(2):265–283.
59. Zhao L, Liu X, Mao J, Xu D, Munjiza A, Avital E. A novel discrete element method based on the distance potential for arbitrary 2D convex elements. *Int J Numer Methods Eng*. 2018;115(2):238–267.
60. Lei Z, Rougier E, Euser B, Munjiza A. A smooth contact algorithm for the combined finite discrete element method. *Comput Part Mech*. 2020;7:807–821.

61. Zheng F, Zhuang X, Zheng H, Jiao Y-Y, Rabczuk T. A robust potential-based contact force solution approach for discontinuous deformation analysis of irregular convex polygonal block/particle systems. *Acta Geotech*. 2020. https://doi.org/10.1007/s11440-020-00997-7.
62. Bao H, Zhao Z. An alternative scheme for the corner–corner contact in the two-dimensional discontinuous deformation analysis. *Adv Eng Softw*. 2010;41(2):206–212.
63. Bao H, Zhao Z. The vertex-to-vertex contact analysis in the two-dimensional discontinuous deformation analysis. *Adv Eng Softw*. 2012;45(1):1–10.
64. Fan H, He S. An angle-based method dealing with vertex–vertex contact in the two-dimensional discontinuous deformation analysis (DDA). *Rock Mech Rock Eng*. 2015;48(5):2031–2043.
65. Wang X, Wu W, Zhu H, Zhang H, Lin J-S. The last entrance plane method for contact indeterminacy between convex polyhedral blocks. *Comput Geotech*. 2020;117:103283.
66. Zhang H, Liu S-G, Zheng L, et al. Method for resolving contact indeterminacy in three-dimensional discontinuous deformation analysis. *Int J Geomech*. 2018;18(10):04018130.
67. Shi G. Contact theory. *Sci China Technol Sci*. 2015;58(9):1450–1496.
68. Cheng X, Xiao J, Wang Y, Miao Q, Xue J. A new and efficient 2D collision detection method based on contact theory. 2016 5th International Conference on Advanced Materials and Computer Science (ICAMCS 2016). Atlantis Press; 2016.
69. Lin X, Li X, Wang X, Wang Y. A compact 3D block cutting and contact searching algorithm. *Sci China Technol Sci*. 2019;62:1438–1454.
70. Doolin DM, Sitar N. Time integration in discontinuous deformation analysis. *J Eng Mech*. 2004;130(3):249–258.
71. Lin S, Xie Z. Performance of DDA time integration. *Sci China Technol Sci*. 2015;58(9):1558–1566.
72. Wang L-Z, Jiang H-Y, Yang Z-X, Xu Y-C, Zhu X-B. Development of discontinuous deformation analysis with displacement-dependent interface shear strength. *Comput Geotech*. 2013;47:91–101.
73. Wang X, Cai M. Modeling of brittle rock failure considering inter- and intra-grain contact failures. *Comput Geotech*. 2018;101:224–244.
74. Wu Z, Fan L, Liu Q, Ma G. Micro-mechanical modeling of the macro-mechanical response and fracture behavior of rock using the numerical manifold method. *Eng Geol*. 2017;225:49–60.
75. Available from: http://www.ddamm.org/wiki/Softwares#DDA_2D.

How to cite this article: Zhuang X, Zheng F, Zheng H, Jiao Y-Y, Rabczuk T, Wriggers P. A cover-based contact detection approach for irregular convex polygons in discontinuous deformation analysis. *Int J Numer Anal Methods Geomech*. 2021;45:208–233. https://doi.org/10.1002/nag.3157